Summer 6-2019

Zinc Chloride Enhanced Chondrogenesis is VEGF Dependent

Gilbert M. Sharp IV
sharpgilbert@gmail.com

Zinc Chloride Enhanced Chondrogenesis is VEGF Dependent

by

Gilbert M. Sharp IV

Submitted in partial fulfillment of the requirements for the degree

Master of Biology

Seton Hall University

June 2019

APPROVED BY

MENTOR

COMMITTEE MEMBER

COMMITTEE MEMBER

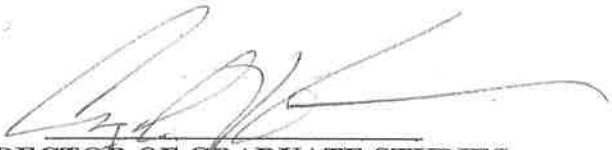

DIRECTOR OF GRADUATE STUDIES

CHAIRPERSON, DEPARTMENT OF BIOLOGICAL SCIENCES

Acknowledgments

This research project was an arduous yet fulfilling journey that resulted in personal growth, many friendships, and many networking connections that will carry me through the next phases of my journey. I am grateful to the Seton Hall University Department of Biological Sciences, Dr. Heping Zhou (Chairperson), Dr. Angela Klaus (Director of the Graduate Program), and Ms. Anjeanette Cook (Secretary) for admitting me into the MS program, appointing me as a Teaching Assistant, providing me with any and all necessary resources, and aiding me in maintaining good status to graduate. I am extremely grateful to Dr. Jessica Cottrell for providing the funding, materials, guidance, patience, motivation, and expertise in her field to allow me to complete this research project. I am grateful for Dr. Cosimo Antonacci and Dr. Angela Klaus for agreeing to be in my thesis defense committee. I am thankful for all the friends and lab mates that helped me persevere, no matter if it was in research or coursework. Finally, I am extremely thankful for my family and friends who gave me the structure outside of Seton Hall and the motivation to finish this thesis.

Table of Contents

List of Tables

List of Figures

Abstract

Researchers have begun investigating whether insulin mimetics such as $ZnCl_2$ could promote bone healing in both non-diabetic and diabetic fracture healing similarly to insulin. Our research focused on understanding the mechanism by which $ZnCl_2$ affects chondrogenesis, an important component of bone fracture healing. The increases in proteoglycan deposition and cell proliferation seen in our data may be a result of $ZnCl_2$ induction of the IGF-1 pathway. When the VEGF pathway was inhibited in $ZnCl_2$- or insulin-treated cells significant decreases in proteoglycan deposition occurred on day 7 and 14 ($P=0.007$ for $ZnCl_2$, $P=0.028$ for insulin) when compared to controls. This data suggests that in the presence of VEGF that Runx1 may be an important mediator in $ZnCl_2$- mediated chondrogenesis. We believe that $ZnCl_2$ may be upregulating many members of the collagen family and BMP-6 which insulin is not. Our data demonstrates that at later timepoints, VEGF inhibition produces higher amounts of genes such as jun, grb2, and cyclin D1 which were identified in the NGS data and confirmed through QPCR. Although the mechanisms by which $ZnCl_2$ and insulin have been shown to overlap, our data suggests that $ZnCl_2$ works through a mechanism different then insulin when employing the VEGF- pathway.

Keywords: bone, fracture healing, chondrogenesis, endochondral ossification, zinc chloride, $ZnCl_2$, insulin, vascular endothelial growth factor, VEGF

Introduction

Diabetes is a disease that affects the metabolism of almost 9.4% of the American population (American Diabetes Association, 2018). Patients afflicted with diabetes typically have delayed or failed bone healing (Graves et. al, 2011). As a result, many studies have focused on developing therapeutics or medicine that could improve diabetic bone fracture healing. A subset of these studies has identified insulin and insulin mimetics such as Zinc Chloride ($ZnCl_2$) as possible therapeutics which can help improve diabetic bone healing (Gandhi et. al, 2005; Wey et. al, 2014; Ovesen et. al, 2001). Although the positive role insulin plays on fracture healing is relatively well understood, the mechanism by which insulin mimetics like $ZnCl_2$ promote bone formation is unclear. Therefore, this study aims to characterize the mechanism by which the insulin mimetic $ZnCl_2$ affects chondrogenesis, an important process of bone development and repair.

Bone Development

Bone development is crucial to the survival of multicellular organisms with a skeletal system. Deletion of key genes involved in skeletal development prevents or reduces the viability of the organisms' offspring. Cbfa1 (core-binding factor a1) is a transcription factor that signals mesenchymal cells to differentiate into osteoblasts. In fact, Cbfa1 null mice die quickly upon birth and are unable to convert their precursor cartilaginous skeleton into bone (Komori et. al, 1997). Bone development begins when the somite lineage gives rise to the axial skeleton, next the lateral plate mesoderm lineage gives rise to the limb skeleton, and finally the cranial neural crest generates the cartilage branchial arch and craniofacial bones (Gilbert SF, 2000). Primary bone formation occurs

through a process of intramembranous ossification. Intramembranous ossification involves the direct formation of bone from mesenchymal cells, with no cartilage intermediate. Secondary bone formation or endochondral ossification occurs when mesenchymal stem cells (MSCs) become cartilage cells and form the bony frame of cartilage.

Endochondral ossification is initiated when mesenchymal stem cells are committed to becoming chondrocytes. Two paracrine transcription factors, Pax1 and Scleraxis aid this transition by stimulating genes specific to chondrocyte differentiation (Sosic et. al, 1997; Cserjesi et. al, 1995). The Sry-homeobox 9 (SOX9) gene is another important gene expressed in the pre-cartilaginous condensations of MSCs. Without SOX9 expression, humans can develop campomelic dysplasia, a rare and severe bone disorder that affects most bones throughout the body. This condition causes a weakening of the cartilage, which especially affects the upper respiratory tract, a condition called laryngotracheomalacia (NIH- Campomelic dysplasia, 2014; Wright et. al, 1995). Liao et al. demonstrates that Sox9 can mediate bone morphogenic protein-2 (BMP-2) induced MSC differentiation into chondrocytes and promote the formation a cartilaginous skeletal precursor (Liao et. al, 2014). During this process the perichondrium is invaded by capillaries and it is transformed into the periosteum (Wang et. al, 2017). Chondrocytes in the area differentiate, swell, and become hypertrophic. Chondrocytes become hypertrophic due to many factors, two of which include a change in respiration metabolism and a secretion of membrane-bound vesicles. When chondrocyte respiration changes from aerobic to anaerobic, partly due to creatine kinase, it leads to an altered

mitochondrial energy potential, an altered cell metabolism, and hypertrophy (Shapiro et. al, 1992).

Chondrocytes that have undergone hypertrophy secrete membrane-bound vesicles into the matrix of the fracture site; these vesicles release enzymes that generate a molecular cocktail of calcium phosphate that is rich in acid-phosphate, annexin V, lipid mediators, and signaling proteins. Once released, these molecules aid in mineralization of the cartilage matrix (Wu et. al, 1997). Following hypertrophy, chondrocytes undergo tumor-necrosis factor alpha (TNF-α) induced apoptosis which leads to cartilage matrix mineralization, characterized by collagen X and fibronectin deposition (Bruder and Caplan, 1989). Macrophage colony stimulating factor (M-CSF), osteoprotegerin (OPG), tumor necrosis factor alpha (TNF-α), and receptor activator of nuclear factor kappa B ligand (RANKL) stimulate the resorption of the mineralized cartilage; during this time, RANKL, M-CSF, and OPG are thought to help bone cells create woven bone (Gerstenfeld et. al, 2003). The vasculature that is formed allows for precursor osteoblasts to migrate into the bone forming region. Once mineralized, blood vessels penetrate the bone site, and osteoblasts utilize the cartilage scaffold to form new bone (Gilbert SF, 2000). A summary of the gene and proteins influencing endochondral ossification during bone development is shown in Figure 1. (Goldring et. al, 2006).

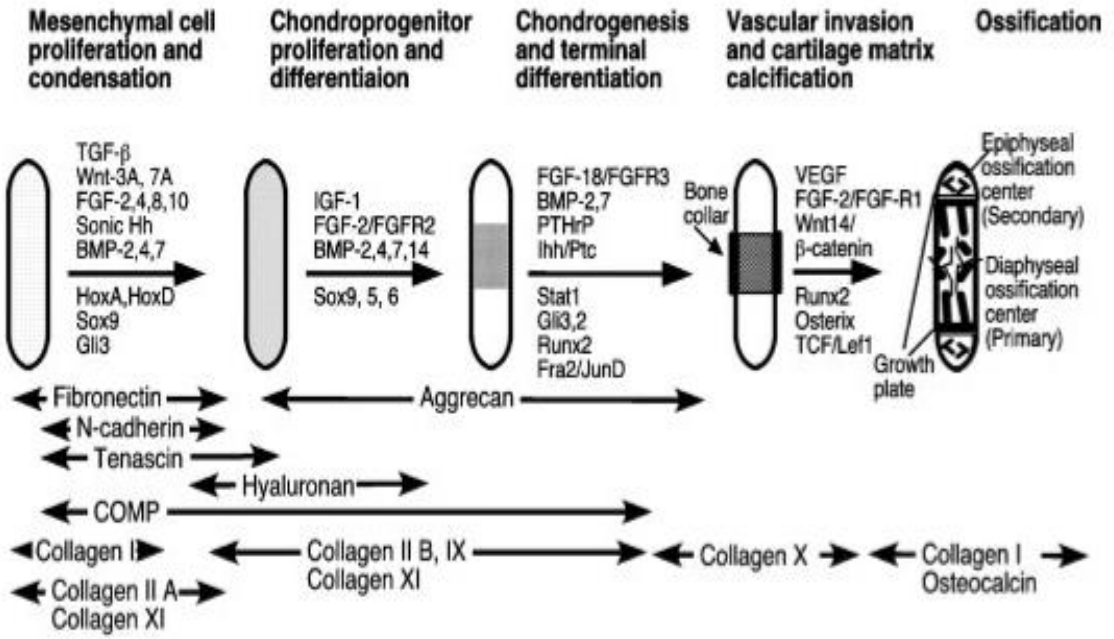

Figure 1: Sequence of events during the development of long bones (Goldring et. al, 2006). In this figure, the major protein and gene interactions are shown as corresponding to the stage of the bone development process. As bones develop, first the mesenchyme proliferates and condenses due to genes that include sonic hedgehog (SHH), transforming growth factor β (TGF-β), and Sox9. The proteins involved in this stage include collagens I, IIA, and XI. When chondroprogenitor cells begin to proliferate and differentiate into chondrocytes, insulin like growth factor 1 (IGF1), bone morphogenetic proteins 2,4,7,14 (BMP-2,4,7,14), and Sox9,5,6 are active. Hyaluronan and collagens IIB, IX, and XI are active in this stage. The protein aggrecan is made in this stage and continues into chondrogenesis and chondrocyte hypertrophy. Runt transcription factor x2 (Runx2), BMP2,7, fibroblast growth factor (FGF18, FGFR3), Indian hedgehog, and junD are involved in chondrogenesis and hypertrophy. Vascular endothelial growth factor (VEGF), runx2, FGF2, FGFR1, osterix, and β-catenin are among the major genes involved in vascular invasion and cartilage mineralization. The proteins involved here are solely collagen X, indicating bone is beginning to become finalized. In the final ossification stage, gene transcription to aid the fracture healing is reduced significantly and collagen I and osteocalcin are the major proteins used to completely heal the bone.

Fracture Healing

Most fractures heal through secondary bone healing and progress through distinct phases including inflammation and hematoma formation, soft tissue callus formation, callus mineralization, and bone remodeling. Day 0-3 involves initial hematoma and inflammation with monocytes, T-cells, macrophages, polymorphonuclear neutrophils (PMN or granulocytes), and B-cells. Day 3-5 involves the hematoma stage but the bone marrow stem cells (BMSCs) are the major mediator. Through the help of osteoblasts and chondrocytes, days 5-10 are characterized by a soft callus with unmineralized cartilage. Days 10-16 involve chondrocyte hypertrophy and osteoclasts that form the fibrous bone tissue. During days 16-21, hematopoietic cells and myelopoietic cells are active that form hard callus, also known as secondary bone. With the aid of osteocytes, days 21-35 finalize the fracture healing process into remodeled bone (Wang et. al, 2017).

Immediately following fracture, inflammation floods the site of damage and leads to hematoma formation. The hematoma is comprised of blood cells and bone marrow cells including macrophages, B cells, and T cells, coagulating in response to inflammation. This coagulation provides a scaffold for the soft tissue callus to form around (Gerstenfeld et. al, 2003). Cells of the primary inflammatory response secrete many proinflammatory molecules including TNF-α, interleukin-1 (IL-1), IL-6, and IL-11. These molecules encourage angiogenesis and spur the influx of more inflammatory cells to the site of the fracture (Sfeir et. al, 2005). TNF-α is expressed by these inflammatory cells, leading to chemotaxis of other required cells such as neutrophils, macrophages, B cells, and T cells (Zhang et. al, 2009). In addition, IL-1 secreted by macrophages induces

IL-6 production in osteoblasts, elevates angiogenesis at the fracture, and aids in the construction of the primary cartilage callus (Kon et. al, 2001). Secretion of IL-6 can stimulate angiogenesis, the production of VEGF, and allow osteoclasts and osteoblasts to differentiate (Yang et. al, 2007). IL-11 has been shown to increase bone formation and prevent cortical bone loss, as well as increase osteoblast differentiation in the presence of BMP-2 (Takeuchi et. al, 2002).

The recruitment of mesenchymal stem cells is crucial to fracture healing and is stimulated by many factors including SDF-1, CXCR4, TGF-B, BMPs, and Runx2 (Granero-Molto et. al, 2009). Data has demonstrated a relationship between stromal cell derived factor 1 (SDF-1) and CXCR4, the G-protein coupled receptor of SDF-1 exists. These factors work together to regulate the influx of mesenchymal stem cells to the site of trauma. When SDF-1 was overexpressed in a methylprednisolone induced osteonecrosis femoral head rat model, fracture healing was improved due to an increase in osteogenesis and angiogenesis (Yang et. al, 2018). Data has also shown that only mesenchymal stem cells that express the CXCR4 receptor can navigate themselves to the fracture callus (Kitaori et. al, 2009). BMP-7, and other BMPs, are also thought to orchestrate the recruitment of bone progenitor cells to the fracture; BMP-2 has been shown to be crucial for osteogenesis but does not have a role in osteogenic cell recruitment (Bais et. al, 2009).

Once the mesenchymal cells are recruited many of them differentiate into chondrocytes and begin producing, collagen I and collagen II in the matrix. The TGF-β superfamily, specifically TGF-β2 and β3, as well as GDF-5 are of high importance in the

chondrogenesis and endochondral ossification (Cho et. al, 2002). TGF-β has been shown to stimulate mesenchymal stem cells to proliferate and differentiate into chondrocytes early in the fracture healing process (Joyce et. al, 1990). Runt transcription factor isoform 2 (Runx2) is a major regulator of chondrocyte proliferation and differentiation during endochondral ossification. Runx2 null mice are unable to undergo endochondral ossification necessary for bone formation and result in nonviable offspring (Chen et. al, 2014). Mice that were specifically floxed for a deletion of Runx2 in $Runx2^{\Delta E8/\Delta E8}$ mice were unable to produce mature chondrocytes or vasculature (Chen et. al, 2014). Runx2 is a direct regulator of genes controlling the cell cycle, including cyclin A1 and c-Myb which has been linked to its ability to regulate the proliferation of chondrocytes (Chen et. al, 2014).

Once chondrocytes become hypertrophic, they express Osterix (Osx) and being to produce copious amounts of VEGF; this leads to a recruitment of chondroclasts into the fracture site (Carlevaro et. al, 2000). In studies, where exogenous VEGF was added during fracture repair, healing improved (Peng et. al, 2002). When Sprague-Dawley rats received TNP-470, a VEGF inhibitor, their unilateral closed femoral fractures resulted in non-unions due to the lack of vasculature from the inhibitor; uninhibited rats did not have adverse fracture healing. Another study involved a cylindrical defect being drilled into Sprague-Dawley rats and an adenoviral vector was added to encode VEGF; the other animals received no intervention. Healing was promoted in the animals that received the VEGF treatment and their bone mineral content was also enhanced over the non-treated control mice; VEGF treated mice in this experiment also completed the endochondral

phase of bone development faster. (Keramaris et. al, 2008). VEGF null mice also have delays in blood vessel invasion surrounding the center of primary ossification and delays in removing terminally differentiated chondrocytes from the bone formation site (Berendsen and Olsen, 2014). The role of VEGF in bone healing may also be enhanced through interactions with other pro-angiogenic factors including the BMP family (Deckers et. al, 2002).

In bone repair, new bone must be formed by osteoblasts and old bone must be resorbed and remodeled by osteoclasts. The Wnt family can stimulate mesenchymal stem cells to differentiate into osteoblasts as well as spur on osteoblasts to form new bone (Chen et. al, 2009). VEGF has been shown to influence the function of both osteoblasts and osteoclasts. At the location of the bone damage, VEGF was seen along the new trabeculae but not inside the cells inside of the bone, demonstrating that osteo-lineage cells, including osteoblasts, are crucial producers of VEGF that is necessary to heal cortical damage. A 3D-reconstruction of injured bone showed significantly decreased amounts of mineralized tissue in VEGF-deficient mutants. Osteoblasts from VEGFA knock-out mice had reduced mineralization in culture when compared with controls. VEGF expression on hypertrophic chondrocytes causes monocytes to differentiate into osteoclasts. Also, osteoblast-secreted VEGF allows neutrophils to enter during the acute inflammatory stage (Hu and Olsen, 2016). Once the cartilage is replaced by bone, it is remodeled to increase the stability of the bone. The hard callus is remodeled into lamellar bone with a central cavity, the medulla. The process of remodeling bone is a balance between depositing bone by osteoblasts and resorbing the hard callus by

osteoclasts which is primarily influenced by IL-1, RANKL, and TNF-α (Wendeberg, 1961).

VEGF pathway

VEGF is a signaling molecule that is important for many processes such as vasculogenesis, angiogenesis, and bone repair. VEGF has been identified as a key paracrine agent in vasculogenesis (Carmeliet et. al). VEGF promotes angiogenesis, leads to a rise in permeability of the vasculature, and facilitates the modification of the extracellular matrix (Hoeppner et. al). AP-1 (activator protein 1) is a transcription factor that is responsible for proliferation, increased gene expression, and tumor progression. Overexpression of both mTOR (mammalian target of rapamycin) and AP-1 increase the transcriptional and protein levels of vascular endothelial growth factor. An increase in VEGF leads to improved bone healing. Cottrell et al. demonstrated using an in vitro chondrocyte cell model that $ZnCl_2$ treatment affected mTOR gene expression suggesting that this insulin mimetic may exert its affect by modulating VEGF expression or associated pathways (Burgess and Cottrell, 2017). The TGF (transforming growth factors) family of signaling molecules are known to induce transcription of many genes, including VEGF. TGF-B induces VEGF gene expression through Smad proteins, which encourage transcription through binding with DNA-binding proteins. Hypoxia also greatly increases this property of TGF-B (Sanchez-Elsner T et. al) which is commonly exists during early fracture repair.

Insulin is a widely studied signaling molecule that can increase VEGF's gene expression through its relationship with the HIF-1a (hypoxia inducible factor) and ARNT (aryl hydrocarbon receptor nuclear translocator) complex. Insulin and insulin growth factor-1 (IGF-1) can stabilize the hypoxia response element, increase the expression of Glut1, a glucose transporter (Zelzer et. al) and lead to the overexpression of HIF-1a which stimulate an increase in the release of growth factors IGF-2, IGFBP-2, and IGFBP-3. These have an important role in bone formation and chondrogenesis as they are directly related to the insulin pathway that improves bone formation (Feldser et. al). *Vegfa*$^{fl/fl}$*Osx-Cre/ZsG* mice have a decrease in bone marrow-released neutrophils during the acute phase of inflammation, due to a deleted VEGFA gene (Hu and Olsen, 2016). This data suggests a mechanism by which osteoblast generated VEGF facilities neutrophil proliferation and activation which are cells important to bone processes including chondrogenesis (Hu and Olsen, 2016).

Insulin Signaling and chondrogenesis

Insulin signaling is a crucial component of chondrogenesis as well as other stages of the bone healing process (Vardatsikos et. al, 2013). Insulin is a hormone that influences the metabolism of bone and fracture healing, among many physiological phenomena. The insulin receptor is a family of receptor tyrosine kinase signaling proteins

that are transmembrane. This family includes the classical insulin receptor and insulin-like growth factor receptors 1 and 2.

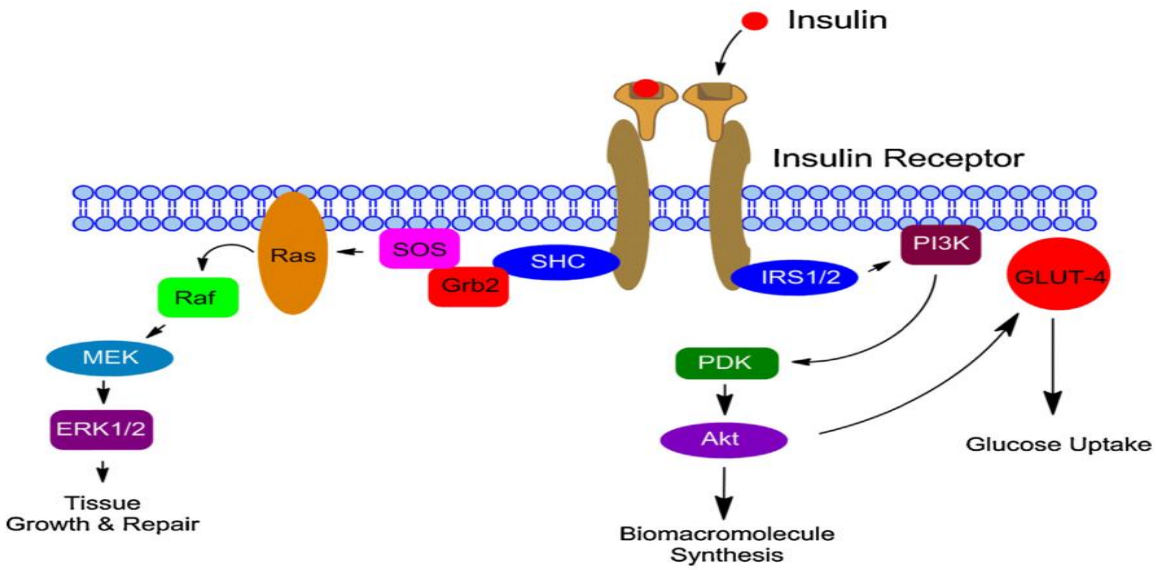

Figure 2: Insulin receptor and the major signaling pathways used in tissue repair (Hrynyk et. al, 2014). This figure depicts the three major outcomes of the canonical insulin receptor and the pathway mediators that are utilized. When insulin binds to the insulin receptor, SHC binds to Grb2, allowing SOS to activate the Ras pathway. Ras activates Raf, which activates MEK, which activates ERK1/2, allowing for tissue growth and repair. When insulin binds to the insulin receptor, IRS1/2 allows for PI3K to activate PDK, which activates Akt. Akt activation allows for direct biomacromolecule synthesis. Akt activation also allows for GLUT4 activation, which increases glucose uptake. This increase in glucose levels provides the cell with the energy to repair the damaged tissue.

The classical insulin receptor is constructed as a pro-receptor and then is cleaved to form a hetero-tetrameric receptor. This receptor is composed of two alpha subunits and two beta subunits, linked in a β-α-α-β configuration by disulfide linkages; the receptor has two monomers, each with one alpha and one beta subunit (Bravo et. al, 1994). The alpha subunits are the extracellular domain and the beta subunits contain the transmembrane domain, the tyrosine kinase domain, an ATP binding site, and a tyrosine auto phosphorylation site (Fantl et. al, 1993). In the course of insulin receptor activation,

insulin binds to one of the two binding sites on each of the monomers, named sites 1 and 2. When insulin binds to site 1, cross linking occurs that allows site 2 to be available for binding, which allows the receptor to be activated (Becker and Rother, 1990). Usually the alpha subunit blocks the ability of the B subunit to auto-phosphorylate, but once insulin is bound the alpha subunit cannot achieve this blocking; therefore, the kinase activity of the beta subunit can now trans-phosphorylate, change its conformation, and increase its kinase potential. The classical insulin receptor and IGF-1 receptors can produce functional hybrid receptors, demonstrating why IGF-1 and classical insulin can interact with the other's receptor (Patti and Kahn, 1998).

Once receptor dimerization occurs, signal transduction can ensue. This begins with phosphorylation of tyrosines located on intracellular B- subunits on the insulin receptor. These phospho-tyrosines are not able to function as a docking site. This permits the Src homology and collagen (SHC) protein to bind to the kinase through their Src-homology-2 domains. This signal is now continued through growth factor receptor bound protein 2 (Grb2), son of sevenless (SOS), and Ras. Ras then propagates the signal through Raf, MEK, and ERK. ERK, and finally can translocate into the nucleus. Once inside the nuclear membrane, ERK can cause the cell to proliferate. This signaling pathway has an effect that aids in wound healing and tissue repair, including bone fracture healing (Saltiel and Kahn, 2001).

The activation of the insulin receptor also stimulates glucose uptake and the synthesis of biomacromolecules, which are crucial in facilitating tissue repair. Once tyrosines are phosphorylated, insulin receptor substrates 1 and 2 can bind to the receptor

and propagate signal transduction through the PI3K/phosphoinositide dependent protein kinase (PDK)/Akt pathway. This allows for the breakdown of fats and creation of glycogen and structural proteins, aiding in repairing tissue damage and providing energy for cell proliferation. The activated Akt pathway also aids in glucose uptake due to glucose transporter type 4, GLUT4 (Pessin and Saltiel, 2000). Phospho-Akt can also lead to increased blood flow, angiogenesis, and cell survival through endothelial nitric oxide synthase, eNOS (Lima et. al, 2012). Insulin's effect on wound healing is still not fully elucidated, but the literature demonstrates that the insulin signaling can orchestrate biomacromolecule procurement and tissue regeneration (Hrynyk et. al, 2014).

Poor diabetic fracture healing is postulated to stem from decreased insulin signaling, which plays critical roles in signal transmission from glucose uptake to tissue repair and growth (Jiao et. al, 2015). Several studies have concluded that localized insulin administration can enhance fracture healing in both diabetic and non-diabetic animals (Paglia et. al, 2013). In an in-vivo murine load-bearing defect model, injected with insulin an increase in osteoblast number was found with a concomitant increase in osteoid area (Dedania et. al, 2011). Insulin treatment in vitro has been demonstrated to stimulate chondrocyte proliferation and differentiation. More specifically, gene expression of collagen 2a1 and glycosaminoglycan were upregulated, demonstrating insulin's ability to increase chondrocyte differentiation and proliferation (Iwata et. al, 2010). Lee et al also demonstrated that local insulin treatment increased mineralization at 4 and 6 weeks using an osteotomy model (Lee and Pilch, 1994). Rat osteoblasts have also been shown to have functional insulin receptors that increase collagen production

when activated by insulin in vitro (Cornish et. al, 1996). Finally, Mueller's study in mesenchymal stem cells demonstrates that glycosaminoglycan production increased in a dose-dependent manner after insulin treatment (Mueller et. al, 2013). These data demonstrate that insulin is a regulator of chondrogenesis and collagen production during bone healing.

Zinc and Chondrogenesis

Zinc chloride ($ZnCl_2$) treatment has been demonstrated to aid in bone healing (Vardatsikos et. al, 2013). An insulin mimetic is a substance that gives an insulin-like effect but does not lead to the fat buildup the insulin causes. Zinc is stored in the pancreas just like insulin which encouraged the idea initially that it was an insulin mimetic (Howell et. al, 1969). $ZnCl_2$ was determined to be an insulin mimetic in 1980 when an experiment demonstrated its ability to mimic insulin's ability to increase fat production in rat adipocytes (Sakurai et. al, 2002). Zinc can function as an intracellular signaling molecule and it has a role in many processes including growth and development (Tudor et. al, 2005). Zinc can enhance the phosphorylation of tyrosine kinases, which includes the classic insulin receptor, insulin-like growth factor type-1 and 2 receptors (IGF1R and

IGF2R, Figure 2).

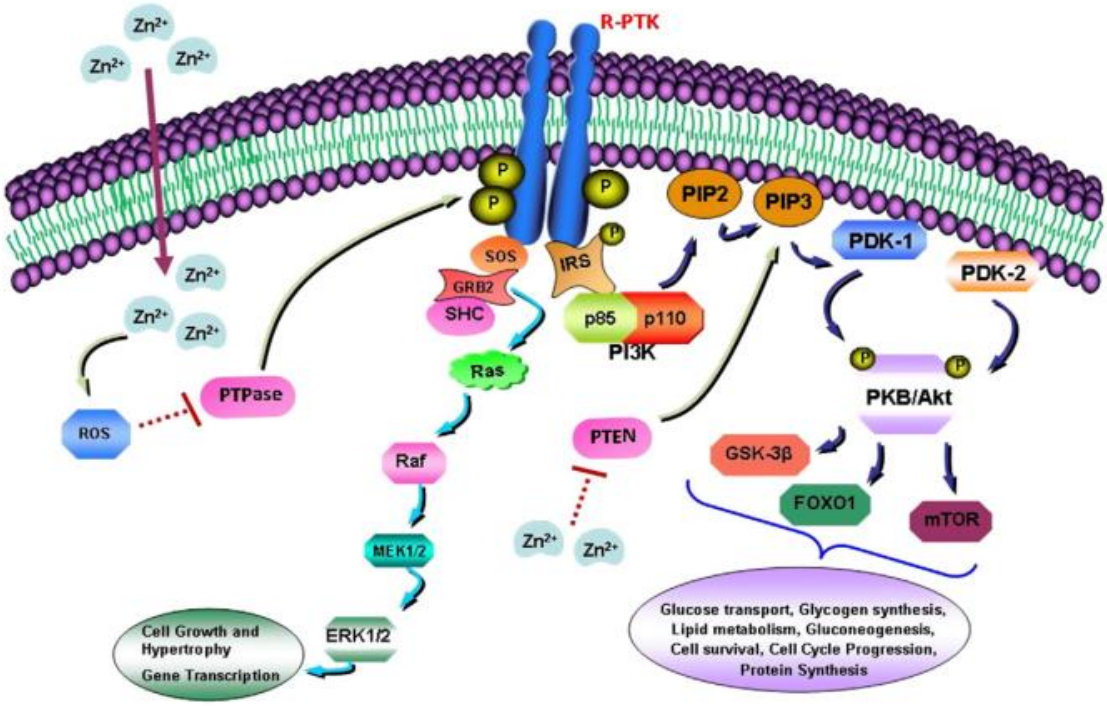

Figure 3: The potential mechanism for the insulin-like effects of zinc (Vardatsikos et. al, 2013). Zinc is a divalent ion that can enter the cell through the lipid membrane. It causes increased activation of tyrosine phosphatases, which lead to end gene upregulation of ERK1/2 and PKB/Akt.

Zinc elicits this effect partly through causing a rise in reactive oxygen species that lead to an increase activation of tyrosine phosphatases, which further phosphorylates tyrosines on protein tyrosine kinases. Activated protein tyrosine kinases then phosphorylate downstream targets including substrates of the insulin receptor, which can lead to activation of the MAPK/ERK signaling pathway as well as the phosphoinositide 3 kinase (PI3K)/protein kinase B (PKB)/AKT signaling pathway. The ERK pathway leads to an increase in gene transcription, cell growth, and hypertrophy. The PKB/AKT pathway, based on its downstream targets, which include mammalian target of rapamycin

(mTOR) and forkhead box protein O1 (FOXO1), causes an increase in protein synthesis, cell cycle progression, cell survival, gluconeogenesis, lipid metabolism, glycogen synthesis, and glucose transport (Vardatsikos et. al, 2013). Zinc regulation has also been demonstrated partially to be controlled by metallothionein proteins. The role of metallothioneins in zinc-induced differentiation and proliferation has been related to modulation of second messenger metabolism, cellular signal recognition, protein phosphatase and kinase activity, and the ability to stimulate or inhibit transcription factors (Beyersmann and Haase, 2001).

Many forms of zinc have been shown to affect bone healing responses both in vitro and in vivo. For instance, $ZnCl_2$ has been shown to activate phospho-AKT and promote chondrocyte maturation in the ATDC5 in vitro chondrocyte cell model (Burgess and Cottrell, 2017). $ZnSO_4$ treatment also increased the number of vascular endothelial cells through the lipoxygenase pathway, which operates through endogenous basic FGF. This leads to a better bone healing outcome, due to more vasculature, which accelerates the fracture healing process (Kaji et. al, 1994). While zinc calcium sulfate treatment increased bone density as measured with by microCT in a rat spinal fusion model (Koerner et. al, 2016). In a Wistar rat model, $ZnCl_2$ local release through a calcium sulfate carrier has been shown to enhance chondrogenesis through histologic analysis (Krell et. al, 2017). Zinc acexamate was shown to significantly increase the amount of IGF-1 and TGF-β over control, further demonstrating the impact that zinc compounds have on enhancing fracture healing (Igarashi and Yamaguchi, 2001). The mechanism by which $ZnCl_2$ and other zinc compounds have on enhancing fracture healing in diabetic

and non-diabetic is unclear (Sakurai et. al, 2002). Further research to determine this mechanism is warranted.

Hypothesis and purpose

The overall purpose of this research is to investigate the molecular mechanism by which the insulin mimetic, zinc chloride elicits positive effects on chondrogenesis. More specifically, the below research hypothesizes that zinc chloride treatment increases VEGF expression in chondrocytes which enhances their proliferation and function. These positive effects on chondrogenesis could contribute to the enhanced healing seen in zinc chloride treated fracture healing models.

Materials and Methods

Cell Culture Methods

ATDC5 cells were utilized for this project as they are a chondrogenic cell line. They are utilized in research to demonstrate and model how chondrocytes differentiate. They were originally isolated from the AT805 teratocarcinoma cell line of differentiating stem cells.

ATDC5 cells were grown in growth media, containing DMEM/F12 50:50 (Dulbecco's Modification of Eagle's Media) supplemented with 5% fetal bovine serum and 1% penicillin-streptomycin, glutamate, transferrin, and selenium. The cells were grown in a 37°C & 5% CO_2 incubator.

RNA Isolation and Quantification

Confluent ATDC5 cells were placed in growth media supplemented with 1ug/mL insulin, 0uM zinc chloride, or 100uM $ZnCl_2$ to stimulate differentiation. Cells were treated for 24 hours and RNA was collected with a RNeasy Mini Kit (Qiagen, Hilden, Germany) using the manufacturer's directions. Quality and quantity of RNA was determined using a BioDrop spectrophotometer (BioDrop, Cambridge, United Kingdom). The RNA concentration was determined by 260 nm absorbance and calculated by the BioDrop device. The RNA quality was verified using the 260/280 absorbance ratio. Samples of these calculations can be found in Table 1 in Appendix. A sample calculation of RNA quality is shown below:

Sample Name and Timepoint: Growth Media 1 Day 4. A260 = 0.359. A280= 0.176. A260/A280 = 2.040.

An aliquot of resulting RNA was separated by gel electrophoresis in a 1% agarose gel made with 3-morpholinopropane-1-sulfonic acid (MOPS) buffer and diethyl pyrocarbonate (DEPC) RNase free water. The gel underwent electrophoresis at 90V for 1 hour and stained with either SYBR GreenGlo (ThermoFisher Scientific, Waltham, Massachusetts) or ethidium bromide (0.1 ug/ml). The gel was then visualized on a Protein Simple FluorChem E machine (Protein Simple, San Jose, California) under the SYBR Green settings and an image was captured. Only RNAs with acceptable characteristics including RNA bands located at 16S (900 bases) and 28S (1800 bases) ribosomal RNA were used for further analysis in RNA Deep Sequencing or Quantitative Real Time Polymerase Chain Reaction (PCR).

RNA Deep Sequencing & Data Generation

Total RNA isolates were purified to isolate the mRNA fraction using a GeneRead Pure mRNA kit by Qiagen (Qiagen, Hilden, Germany) following the manufacturer's instructions. The purified mRNA was quantified afterwards using the BioDrop spectrophotometer (BioDrop, Cambridge, United Kingdom) and sent to the Molecular Research Facility (MRF) at Rutgers Newark for RNA Deep Sequencing (Rutgers University- Newark Campus, Newark, NJ).

At the MRF the samples were purified and quantified, as needed prior to sequencing. Sequencing was completed using an Illumina NextSeq 500 (Illumina, San Diego, California). NGS data was received and analyzed in CLC Genomics Workbench by aligning raw reads to an updated *Mus musculus* reference genome, GRCm38 (NCBI GRC). Samples were run on a High flow cell at a 1x75bp configuration. RPKM normalized gene expression values and fold changes (between all treatment groups) were determined for each gene and 1-way analysis of variance (1-way ANOVA) was utilized to determine any statistical differences between treatment groups, where significance was determined by a $P<0.05$. Graphical plots were created for these in SigmaPlot 13 (Systat Software, San Jose, California).

Ingenuity Pathway Analysis (IPA) by Qiaqen (Qiagen, Hilden, Germany) was used to predict pathway regulators based on fold gene expression changes amongst the treatment groups. The transformed RPKM (reads per kilobase per million) value of insulin was normalized against the transformed RPKM of growth media by the

ratio $\frac{transformed\ RPKM\ \ insulin}{trandformed\ RPKM\ growth\ media}$ and the transformed RPKM of $ZnCl_2$ was normalized the same way. Once these normalized ratios were derived, a core analysis was conducted separately for both $ZnCl_2$ and insulin treatment groups. Each treatment group had effector networks and association networks created for their data set.

Once the core analyses were completed, a comparison analysis was run to compare the two treatment groups. The comparison analysis then took the transformed RPKM ratios for both insulin and $ZnCl_2$ and overlaid them onto canonical pathways to determine which treatment had a significant increase or decrease in the utilization of that specific pathway. The pathways and their fold change increase or decrease, in Z score format, was compared and a $-2 \geq Z \geq 2$ was considered significant by the program. These Z scores can be found in results Table 3. Three selected canonical pathways were chosen to develop RT-qPCR targets, as they were differing with statistical significance between the two treatment groups and had overlaps between the pathways: VEGF Family Ligand-Receptor Interactions, IGF-1 Signaling, and GM-CSF signaling. The Ingenuity Pathway Analysis for GM-CSF signaling can be found in Appendix 3.

Real Time-quantitative PCR

RNA isolation

All RNA isolates were prepped as described previously under RNA isolation and quantification.

Reverse Transcription

RNA was then reverse transcribed (RT) to complementary deoxyribonucleic acid (cDNA). For each reaction, 1ug of RNA, 500uM dNTPs (Thermofisher, Waltham, Massachusetts), 5uM oligo(dT) primer (Thermofisher, Waltham, Massachusetts), and deionized water were combined in a 20ul reaction. The contents were mixed and centrifuged down. The tubes were placed on a 65°C for 3 minutes to disrupt secondary structures and then returned to ice to prevent renaturing of RNA molecules. Next, 2uL of 10X RT Buffer (250mM Tris-HCl, 375mM KCl, 15mM MgCl2, 50mM DTT) (Promega, Madison, Wisconsin), 1uL units of RNAseOUT RNase inhibitor (Thermofisher, Waltham, Massachusetts) and 1uL of MM-LV reverse transcriptase enzyme (Promega, Madison, Wisconsin) were added to the RT reactions and incubated at 42°C for 1 hour. After the 60 minutes incubation, the RT reactions were inactivated by heating at 95°C for 10 minutes. The tubes were then stored in a -20°C freezer.

PCR Procedure

PCR was used to confirm that the reverse transcription procedure successfully produced cDNA. A total volume of 25uL for each PCR reaction was achieved by adding 2.5uL of cDNA template, 2.5uL of 10X Taq buffer (1X in reaction: 10mM Tris-HCl, 50mM KCl, 1.5mM $MgCl_2$, pH 8.3 @ 25°C) (New England BioLabs, Ipswich, Massachusetts), 2.5uM of each primer, 2uL of 5mM dNTPs (Thermofisher, Waltham, Massachusetts), 14.5uL of deionized (DI) water (Millipore Sigma, Darmstadt, Germany), and 1uL of Taq DNA polymerase enzyme (New England BioLabs, Ipswich, Massachusetts). The amount of endogenous cDNA template utilized in the PCR was

derived from 0.1ug of total RNA from the RT reaction. The reaction was run using a forward primer GAGCTGAACGGGAAGCTCACTGG and a reverse primer TCCACCACCCTGTTGCTGTAGCC of glyceraldehyde 3-phosphate dehydrogenase (GAPDH) primer set and using the conditions below on T100 Thermacycler (Applied Biosystems ThermoFisher, Waltham, Massachusetts).

1) 95°C hold for 5 minutes

2) 40 cycles of 95°C denaturation for 30 seconds, 57°C annealing for 30 seconds, and 72°C elongation for 30 seconds

3) 72°C final hold for 10 minutes.

An aliquot of the PCR product was mixed with 5ul loading dye and separated on a 2% agarose gel was made with 1X tris-borate-EDTA buffer (TBE) to ensure integrity of the cDNA and the ability of the cDNA made in each RT reaction to be amplified by PCR. The gels were stained with ethidium bromide (0.1ug/ml), visualized, and photographed on a Protein Simple Fluorchem E machine (Protein Simple, San Jose, California). Only samples with the appropriate single cDNA band located at the correct corresponding weight were used for further analysis.

qPCR

The previously discussed verified PCR products then underwent qPCR to determine gene expression for each treatment groups; they were run to optimize temperature for each primer set. The primers for each gene were developed by Integrated DNA Technologies' Primer Design Tool for 2 primers and an intercalating dye

(Integrated DNA Technologies, Coralville, Iowa). The primer sets and annealing temperature used for qPCR can be found in Table 1.

Gene Name	**Primer Set**	**Annealing Temperature (Tm) (°C)**
GAPDH	F- ACCACAGTCCATGCCATCAC	55°C
	R- TCCACCACCCTGTTGCTGTA	
VEGFA	F- TGGTTCTTCACTCCCTCAAATC	55°C
	R- GGTCTCTCTCTCTCTTCCTTGA	
Jun	F- CCAGACTGTACACCAGAAGATG	55°C
	R- CAACCAAAGTGTCTGCTTTCC	
Grb2	F- CTGTCCGTCAAGTTTGGAAATG	57.8°C
	R- CTTCACCACCCACAGGAAATA	
Sox9	F- CCTGGACTGTATGTGGATGTG	57.8°C
	R- TAAGGTCTGTCCGATGTCTCT	
Runx1	F- CAGAGAGGTGCCAAGGATTT	55°C
	R- CCCTGACCAACAGCTTACTT	
Cycd1	F- CAGAGGCGGATGAGAACAAG	57.8°C

	R- GAGGGTGGGTTGGAAATGAA	
Runx2	F- TGGCTTGGGTTTCAGGTTAG	55℃
	R- GGTTTCTTAGGGTCTTGGAGTG	
VEGFC	F- CCACGTGAGGTGTGTATAGATG	57.8℃
	R- CGGACACACATGGAGGTTTA	
Fos	F- ATTGTCGAGGTGGTCTGAATG	54℃
	R- TCGAAAGACCTCAGGGTAGAA	
GMCSF	F- CCAGTTCTTGGAAGGGCTTATT	54℃
	R- TGGAATCTCCTGGCCCTTAT	
Grb10	F- CCCAGAAAGTCTGCTACATACC	57.8℃
	R- GCTGTCAACCATGGCAAATC	
VEGFR2	F- GCGGAGACGCTCTTCATAATA	60.1℃
	R- GACAAGAAGGAGCCAGAAGAA	

Table 1: qPCR primer sets and annealing temperatures

For each qPCR reaction, 25uL of volume was created as follows: 12.5uL of Fast SYBR Green Master Mix (2X), (ThermoFisher, Waltham, Massachusetts), forward and reverse primer at a final concentration of 70nM, diluted cDNA template, and distilled water. Reactions were performed using an Applied Biosystems 7500 real-time

quantitative PCR instrument (Applied Biosystems ThermoFisher, Waltham, Massachusetts) and below thermal cycling conditions.

1) 95°C hold for 15 minutes

2) 40 cycles of denaturing 95°C for 30 seconds, annealing at Tm (°C) determined by primers (found in Table 1) for 30 seconds, and

3) elongation at 72°C for 30 seconds.

Each reaction yielded amplification plot and a melting curve. The amplification plot yielded a C_T, or cycle threshold, where the signal became greater than the noise and the gene expression could be verified. Each reaction's melt curve was analyzed to ensure one specific peak. GAPDH was used as the researcher's control gene, as it is constitutively expressed in every cell, a housekeeper gene. Data was normalized in SigmaPlot 13 (Systat Software, San Jose, California). The method for normalizing the data was derived from Schmittgen et. al's 2008 paper, which can be found in the references. The researcher compared the $2^{-\Delta C(T)}$ values of the growth media control, insulin treated, and zinc treated groups by 1-way ANOVA with a $P<0.05$ significance cutoff. Statistically significant genes were graphed with SigmaPlot 13(Systat Software, San Jose, California) and included in the results section.

Glacial Blue Assay

The Glacial Blue assay, also known as the Alcian Blue assay, is utilized to determine cell proliferation rate by staining the total amount of sulfated glycosaminoglycans. Cells were seeded at density of 50,000cells/well in a 24-well tissue culture treated plate. Once cells were confluent, media was switched to 1ug/mL insulin,

100uM $ZnCl_2$, growth media and axitinib (VEGFR inhibitor) (Pfizer, New York City, NY), 1ug/mL insulin and axitinib, 100uM $ZnCl_2$ and axitinib, or kept in growth media. Treatments were run in triplicate.

Cells were grown for 4 days, 7 days, 10 days, or 14 days and media was changed as necessary. On the specified time point, cell media was removed, and the plates were washed twice with 1X Hank's Buffered Saline Solution (HBSS) (Thermofisher, Waltham, Massachusetts). Cells were fixed, by adding 100% cold methanol to the plate for 5 minutes. Next, the methanol was removed, and the cells were stained overnight with 0.1% Alcian Blue in 0.1M HCl. The cells were then washed three times with 1X HBSS and 300uL of 6M guanidine HCl was added to each well for 24 hours. The absorbance of each plate was read at 595nm on a Molecular Devices SpectraMax M5 spectrophotometer (Molecular Devices, San Jose, California). Absorbance values were used for analysis by 1-way ANOVA and an image of the plate was taken. Absorbance values were then normalized against growth media, the negative control, in order to produce fold changes that were then graphed.

MTT Assay

CO_2 incubator, counted, and then plated at 10,000cells/well in a 96 well tissue culture treated plate. The cells were left in the wells overnight to adhere to the bottom of the well. Cells were then treated with 1ug/mL insulin, 100uM $ZnCl_2$, growth media and axitinib (VEGFR inhibitor), 1ug/mL insulin and axitinib, 100uM $ZnCl_2$ and axitinib, or

kept in growth media. Treatments were run in triplicate and media was changed as necessary. Cells were grown for 1 day, 4 days, 7 days, or 10 days after treatment.

At the specified time point, 10uL of 3-(4,5-dimethylthiazol-2-yl)-2,5-diphenyltetrazolium bromide (MTT) reagent (MTT= 3-(4,5-dimethylthiazol-2-yl)-2,5-diphenyltetrazolium bromide) was added to each of the wells for at least 4 hours, until intracellular purple crystals were seen under the microscope. After incubation, the media and MTT reagent mixture was aspirated off and 100uL of dimethyl sulfoxide (DMSO) was added to each of the wells to be analyzed. After the addition of DMSO, the plate was incubated for 2 hours at room temperature and kept in the dark to protect it from light. Once the 2 hours was completed, the plate underwent spectrophotometric analysis on a Molecular Devices SpectraMax M5 spectrophotometer (Molecular Devices, San Jose, California) and the absorbance for the wells was recorded at 570nm. Absorbance values were collected, and an image of the plate was taken. Absorbance values were then converted to cell proliferation values with the following formula: $\frac{treatment\ group\ absorbance\ value}{growth\ media\ absorbance\ value} \times 100\%$. The cell proliferation values were then analyzed by 1-way ANOVA and a graphical output was obtained.

Data and Statistical Analysis

Graphing and statistical analysis of data between groups was completed using SigmaPlot 13 (SyStat Software, San Jose, California) and appropriate ANOVA and post-testing hoc Holm-Sidak tests.

Results

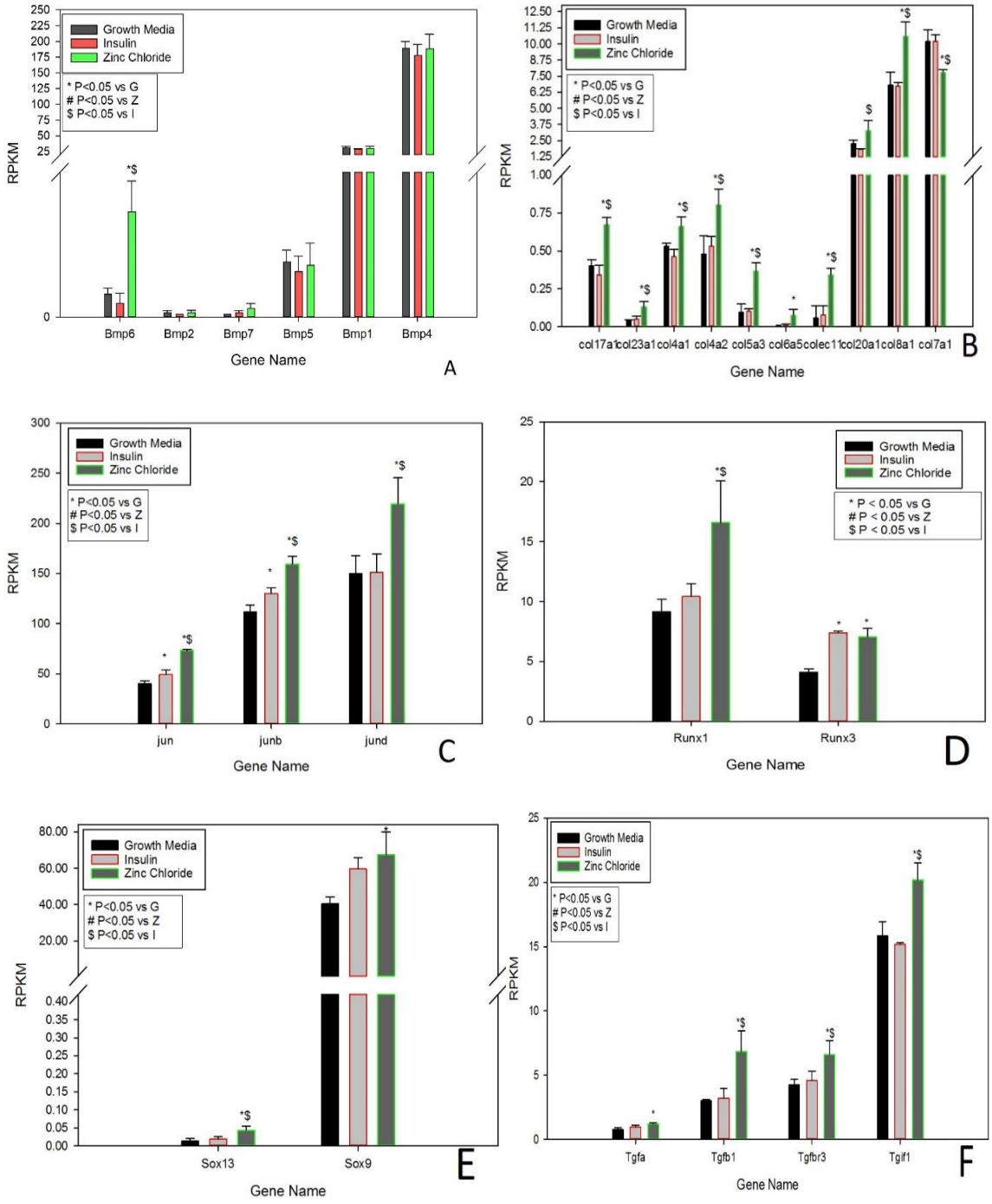

Figure 4: Differential gene expression of $ZnCl_2$-Treated ATDC5 chondrogenic cells 24 hours post-treatment. A) Bone Morphogenetic Proteins (BMPs) B) Collagens C) Jun Family D) Runx family E) Sox Family F) Transforming Growth Factor (TGF)

Superfamily. Each bar graphs compares the transformed reads per kilobase per million (RPKM) of each gene in each treatment group. Statistical significance ($P<0.05$) is denoted each graph and was determined using 1-way ANOVA testing.

For the BMP genes, only BMP6 was found to have a statistically significant difference in RPKM between the treatment groups. $ZnCl_2$ treatment significantly elevated BMP-6 expression by 664% over insulin and 364% over growth media (Figure 4A, Table 2). $ZnCl_2$ treatment significantly elevated the expression of all collagens when compared to media and insulin except for col7a1. The highest percentage increases were in collagen17a1, collagen8a1, collagen ec11, and collagen6a5; collagen6a5 had the highest increase overall for all collagen genes. Collagen17a1 was 96% higher than insulin and 66% elevated over growth media when treated with $ZnCl_2$. When supplemented with $ZnCl_2$, Collagen8a1 had an increase of 54% and 56% over growth media and insulin, respectively. $ZnCl_2$ treated Collagen ec11 expression was 350% and 502% elevated over insulin and growth media, respectively. Collagen6a5's expression when treated with $ZnCl_2$ was elevated by 418% in comparison to insulin and 646% when compared to growth media. In the case of col7a1, $ZnCl_2$ treated gene expression was significantly decreased as compared to insulin and media only groups. Collagen7a1 expression was 24% lower than growth media and 24% lower than insulin when treated with $ZnCl_2$ (Figure 4B).

For jun and junb, both insulin and $ZnCl_2$ were elevated over growth media by 22% and 82%, respectively; $ZnCl_2$ was elevated over insulin by 48% for both genes as well. In the case of jund, insulin had no significant deviation from growth media. However, $ZnCl_2$ treated jund expression was elevated by 46% over both growth media

and insulin (Figure 4C). For the Runx family of genes, both insulin and $ZnCl_2$ treatment groups had a significant increase in gene expression of runx3 by 80% over the negative control, growth media. In the case of runx1, only $ZnCl_2$ had any statistical significance when compared with insulin or growth media (Table 2). $ZnCl_2$ treated ATDC5 cells caused an increase in runx1 gene expression of 59% over insulin and 81% over growth media (Figure 4D).

In the SOX gene family, both SOX9 and SOX13 are upregulated significantly when $ZnCl_2$ treated over growth media while only SOX13 has an upregulation significantly over insulin. For SOX9, $ZnCl_2$ expression is 67% over growth media. For SOX13, $ZnCl_2$ expression is 207% over growth media and 139% over insulin (Figure 4E). For the TGF family of genes, four were demonstrated to show a statistically significant difference in RPKM, as depicted in Figure 4F. $ZnCl_2$ expression was significantly elevated over both growth media and insulin for TGF-B1 (66% over insulin, 75% over growth), TGF-BR3 (45% over insulin, 55.5% over growth), and TGIF-1 (33% over insulin, 28% over growth). For TGF-α, $ZnCl_2$'s expression was only elevated over growth media, at a 58% increase (Figure 4F, Table 2).

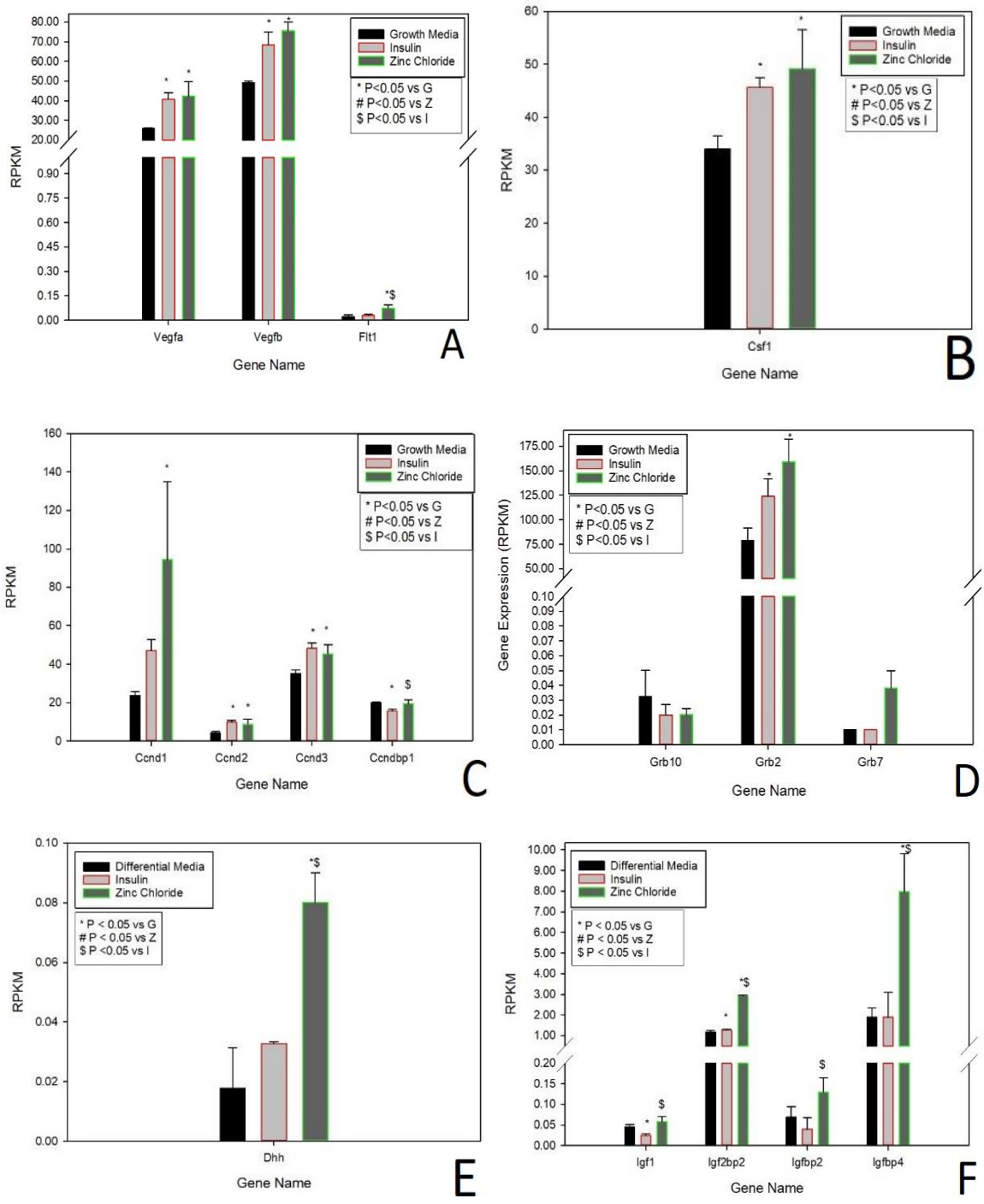

Figure 5: Differential gene expression of $ZnCl_2$-Treated ATDC5 chondrogenic cells 24 hours post-treatment. A) Vascular Endothelial Growth Factor (VEGF) Family B) Colony Stimulating Factor (CSF) C) Cyclin D family D) Grbs E) Hedgehog F) IGFs. Each bar graphs compares the transformed reads per kilobase per million (RPKM) of each gene in

each treatment group. Statistical significance ($P<0.05$) is denoted each graph and was determined using 1-way ANOVA testing.

For the VEGF family of genes, three were demonstrated to show a statistically significant difference in RPKM, as depicted in the above graphic. $ZnCl_2$ and insulin both had elevated gene expression of VEGFA and VEGFB above growth media, 68% and 56% for VEGFA and 58% and 38% for VEGFB respectively. $ZnCl_2$ expression was significantly elevated over both growth media (265%) and insulin (143%) for flt1, a specific pattern only seen in zinc-treated chondrocytes (Figure 5A). For the CSF genes, only Csf1 was demonstrated to show a statistically significant difference in RPKM. $ZnCl_2$ and insulin expression was significantly elevated over both growth media, 45% and 32% respectively (Figure 5B, Table 2).

$ZnCl_2$ expression was significantly elevated when compared to growth media by 300% for cyclin D1, demonstrating a different genetic mechanism in the ATDC5 cell line when treated with $ZnCl_2$ at the 1-day time point as compared to insulin. When ATDC5 cells were exposed to $ZnCl_2$, the gene expression values for cyclin D2 and D3 were 108% and 29% higher than growth media, respectively; insulin treated cells also had this same response, with D2 being 139% elevated and D3 being 37% elevated respectively. In the case of cyclin D binding partner 1, insulin gene expression was decreased by 22% as compared to growth media and $ZnCl_2$ expression was 24.5% increased over insulin (Figure 5C). For the Grb genes, only Grb2 was demonstrated to show a statistically significant difference in RPKM. $ZnCl_2$ had 101.4% increased gene expression over no treatment, growth media, and insulin had 57% elevation above growth media (Figure 5D).

For the Notch Signaling genes, only desert hedgehog (DHH) was demonstrated to show a statistically significant difference in RPKM. $ZnCl_2$ expression was significantly elevated over both growth media and insulin, 371% and 142% respectively, demonstrating a different genetic mechanism in the ATDC5 cell line when treated with $ZnCl_2$ at the 1-day time point as compared to insulin (Figure 5E). In relation to growth media, IGF-1 expression was decreased by 46% when treated with insulin; $ZnCl_2$ expression was elevated by 132% as compared to insulin. When treated with $ZnCl_2$, IGF-binding partner 2 was 233% elevated over insulin. $ZnCl_2$ treatment significantly increased gene expression of IGF-bp4 over insulin by 317% and growth media by 318%. Insulin treatment increased IGF2bp2 expression by 8.7% over growth media; $ZnCl_2$ treatment increased this gene's expression by 130% over insulin and 150% over growth media (Figure 5F, Table 2).

Collagens

Comparison	Diff of Means	t	P	P<0.050
Z-col17a1 vs. I-col17a1	0.329	7.712	<0.001	Yes
Z-col17a1 vs. G-col17a1	0.269	6.294	0.001	Yes
Z col23a1 vs. G col23a1	0.0906	4.693	0.01	Yes
Z col23a1 vs. I col23a1	0.0786	4.075	0.013	Yes
Z col4a1 vs. I col4a1	0.198	4.967	0.008	Yes
Z col4a1 vs. G col4a1	0.129	3.252	0.035	Yes
Z col4a2 vs. G col4a2	0.322	3.987	0.022	Yes
Z col4a2 vs. I col4a2	0.271	3.353	0.03	Yes
Z col5a3 vs. G Col5a3	0.271	7.235	0.001	Yes
Z col5a3 vs. I Col5a3	0.263	7.03	<0.001	Yes
Z col6a5 vs G Col6a5	16.5	3.479	0.037	Yes
Z colec11 vs. G colec11	0.285	5.506	0.005	Yes
Z colec11 vs. I colec11	0.266	5.137	0.004	Yes
Z col20a1 vs. I col20a1	1.441	3.545	0.036	Yes
Z col8a1 vs. I col8a1	3.834	5.285	0.006	Yes
Z col8a1 vs. G col8a1	3.748	5.167	0.004	Yes
G col7a1 vs. Z col7a1	2.416	4.783	0.009	Yes
I col7a1 vs. Z col7a1	2.386	4.723	0.006	Yes

SOXs

Comparison	Diff of Means	t	P	P<0.050
Z Sox13 vs. G Sox13	0.0295	4.189	0.017	Yes
Z Sox13 vs. I Sox13	0.025	3.542	0.024	Yes
Z Sox9 vs. G Sox9	27.111	3.938	0.023	Yes

Runxs

Comparison	Diff of Means	t	P	P<0.050
Z Runx1 vs. G Runx1	7.417	4.118	0.019	Yes
Z Runx1 vs. I Runx1	6.162	3.421	0.028	Yes
I Runx3 vs. G Runx3	3.304	9.128	<0.001	Yes
Z Runx3 vs. G Runx3	2.962	8.184	<0.001	Yes

BMPs

Comparison	Diff of Means	t	P	P<0.050
Z Bmp6 vs. I Bmp6	0.316	5.854	0.003	Yes
Z Bmp6 vs. G Bmp6	0.285	5.284	0.004	Yes

Insulin Like Growth Factors and IGF Binding Partners

Comparison	Diff of Means	t	P	P<0.050
Z-IGF1 vs. I-IGF1	0.0336	5.331	0.005	Yes
G-IGF1 vs. I-IGF1	0.0211	3.35	0.031	Yes
Z-Igf2bp2 vs. G-Igf2bp2	1.753	44.284	<0.001	Yes
Z-Igf2bp2 vs. I-Igf2bp2	1.651	41.701	<0.001	Yes
I-Igf2bp2 vs. G-Igf2bp2	0.102	2.583	0.042	Yes
Z_Igfbp2 vs. I_Igfbp2	0.0911	3.773	0.028	Yes
I_Igfbp3 vs. Z_Igfbp3	221.38	4.3	0.015	Yes
G_Igfbp3 vs. Z_Igfbp3	170.547	3.313	0.032	Yes
Z_Igfbp4 vs. G_Igfbp4	6.058	5.727	0.004	Yes
Z_Igfbp4 vs. I_Igfbp4	6.05	5.719	0.002	Yes
G_Igfbp6 vs. Z_Igfbp6	46.571	4.436	0.013	Yes
I_Igfbp6 vs. Z_Igfbp6	35.512	3.383	0.029	Yes

CycDs

Comparison	Diff of Means	t	P	P<0.050
Z ccnd1 vs G ccnd1	18	3.795	0.02	Yes
I ccnd2 vs. G ccnd2	5.692	3.965	0.022	Yes
Z ccnd2 vs. G ccnd2	4.414	3.075	0.043	Yes
I ccnd3 vs. G ccnd3	13.132	4.774	0.009	Yes
Z ccnd3 vs. G ccnd3	10.166	3.696	0.02	Yes
G ccndbp1 vs. I ccndbp1	4.379	3.829	0.026	Yes
Z ccndbp1 vs. I ccndbp1	3.789	3.313	0.032	Yes

CSFs

Comparison	Diff of Means	t	P	P<0.050
Z csf1 vs. G csf1	15.184	4.025	0.021	Yes
I csf1 vs. G csf1	11.647	3.087	0.042	Yes

Juns

Comparison	Diff of Means	t	P	P<0.050
Z jun vs. G jun	33.28	14.079	<0.001	Yes
Z jun vs. I jun	24.073	10.184	<0.001	Yes
I jun vs. G jun	9.207	3.895	0.008	Yes
Z junb vs. G junb	47.624	8.699	<0.001	Yes
Z junb vs. I junb	29.265	5.345	0.004	Yes
I junb vs. G junb	18.359	3.353	0.015	Yes
Z jund vs. G jund	69.104	4.035	0.02	Yes
Z jund vs. I jund	67.948	3.967	0.015	Yes

TGFs

Comparison	Diff of Means	t	P	P<0.050
Z tgfa vs. G tgfa	0.436	3.904	0.024	Yes
Z tgfb1 vs. G tgfb1	3.8	4.557	0.012	Yes
Z tgfb1 vs. I tgfb1	3.608	4.327	0.01	Yes
Z tgfbr3 vs. G tgfbr3	2.357	3.614	0.033	Yes
Z tgfbr3 vs. I tgfbr3	2.038	3.126	0.04	Yes
Z tgif1 vs. I tgif1	5.005	6.145	0.003	Yes
Z tgif1 vs. G tgif1	4.366	5.362	0.003	Yes

VEGFs

Comparison	Diff of Means	t	P	P<0.050
Z vegfa vs. G vegfa	16.383	4.265	0.016	Yes
I vegfa vs. G vegfa	14.894	3.878	0.016	Yes
Z vegfb vs. G vegfb	26.602	7.011	0.001	Yes
I vegfb vs. G vegfb	19.556	5.154	0.004	Yes
Z flt1 vs. G flt1 (vegfr1)	0.0518	4.714	0.01	Yes
Z flt1 vs. I flt1	0.0431	3.916	0.016	Yes

Grbs

Comparison	Diff of Means	t	P	P<0.050
Z grb2 vs. G grb2	80.091	5.344	0.005	Yes
I grb2 vs. G grb2	44.928	2.998	0.048	Yes

Table 2: Statistically Significant P-Values in the Next Generation Sequencing Experiment. This table contains the statistically significant results of the 1-way ANOVA that was ran on the corrected absorbance values of each treatment group in the Next Generation Sequencing experiment. The table shows the timepoint, the treatments being

compared, the difference of the means, the t score, the P value, and if the P value is less than 0.05, the statistical significance threshold. The letter G signifies growth media, the letter I signifies insulin, and Z signifies $ZnCl_2$.

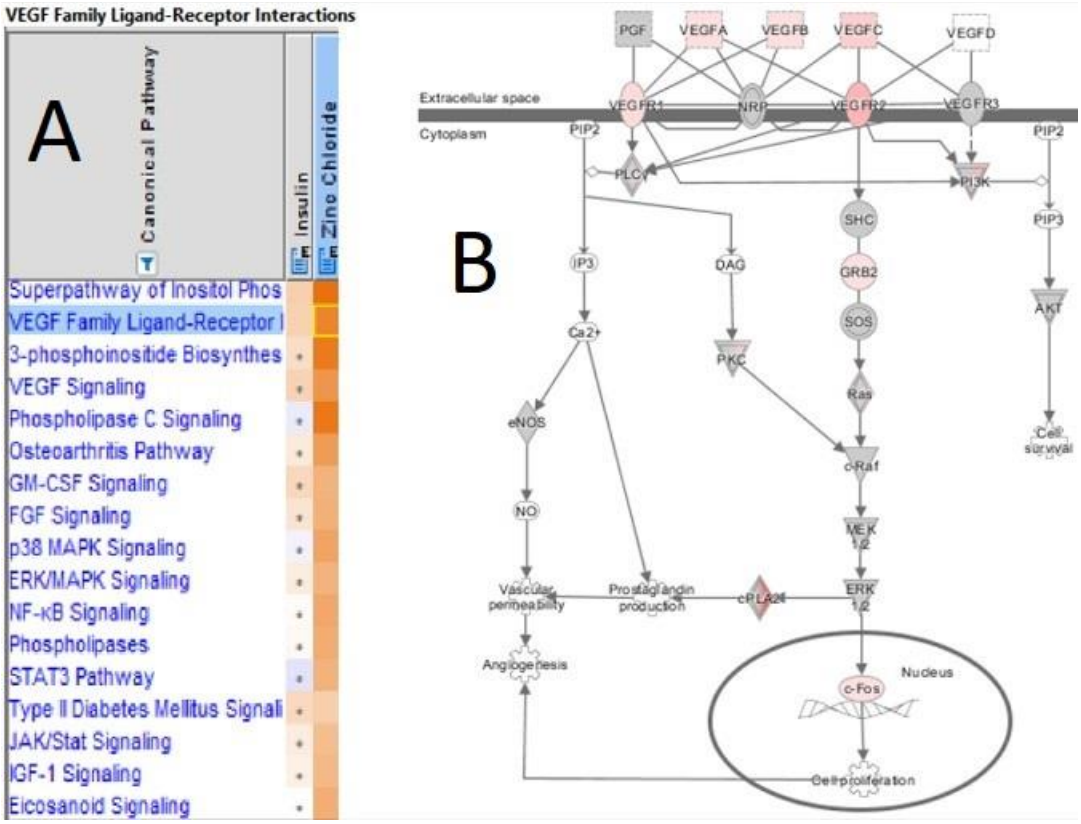

Figure 6: Comparison analysis of gene expression values overlaid onto the VEGF Family Ligand-Receptor Interactions pathway. A) Z score table visualization B) canonical pathway. For A, an orange color indicates a slight upregulation of the pathway and a deeper orange is a strong upregulation of the pathway; a blue color indicates a slight downregulation of the pathway and a deep blue is a strong downregulation of the pathway. A dot in B demonstrates that the result is not statistically significant, where Z is greater than -2 and below 2. A pink color in B indicates slight up-regulation of a gene and a deeper red indicates higher gene expression. A slight green color in B indicates a slight downregulation of the gene and a deep green color indicates high gene downregulation.

In Figure 6, both insulin and $ZnCl_2$ expression values for the genes in the VEGF canonical pathway were compared by Ingenuity Pathway Analysis. This canonical pathway is included as it demonstrates a direct result from the NGS experiment that

shows $ZnCl_2$ is utilizing the VEGF pathway in a different mechanism than Insulin treated ATDC5 cells. $ZnCl_2$ treated ATDC5 chondrocytes have a higher Z score for the VEGF Family Ligand-Receptor Interactions than insulin, as shown in A, where $ZnCl_2$ has a deeper orange. This means that the IPA program utilizes the gene expression values from $ZnCl_2$, compares them to the expected gene values from their algorithm and literature database, and produces the canonical pathway results with those values from their analysis.

The values here in Figure 6B are red, indicating that the expression value of $ZnCl_2$-treated chondrocytes is significantly higher in this pathway than the expression values of insulin-treated chondrocytes as well as being higher than the canonically accepted values. VEGFA-C and VEGFR1-2 are a deep red color, indicating that this pathway is being highly upregulated. c-fos and grb2 downstream are also slightly upregulated.

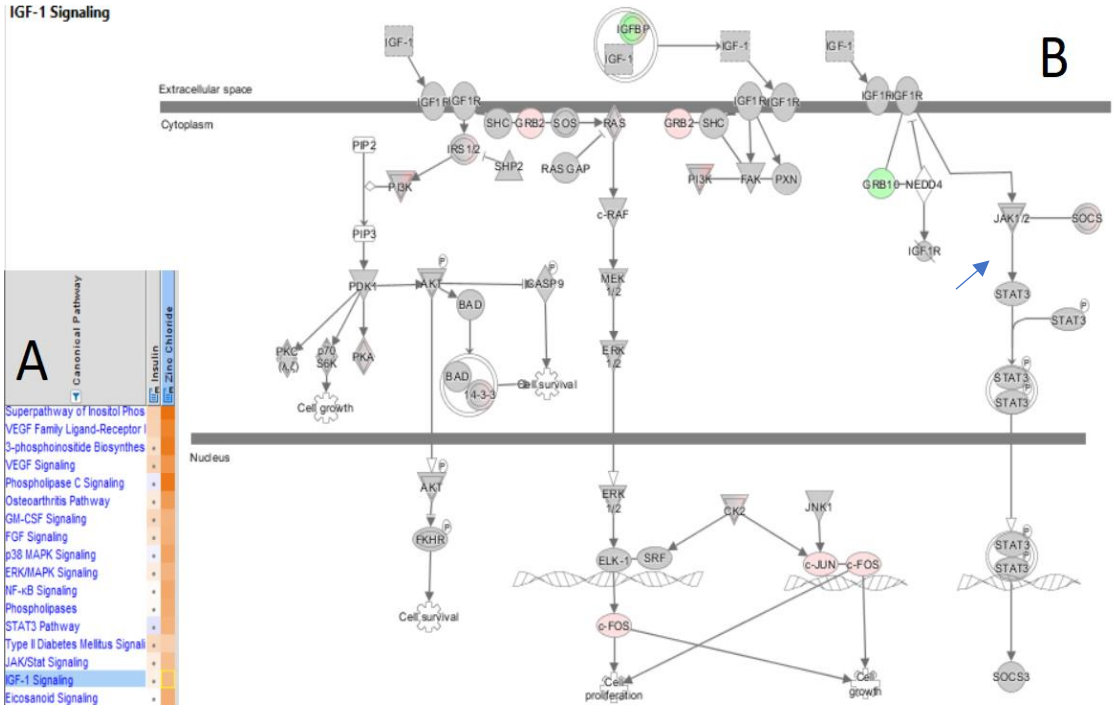

Figure 7: Comparison analysis of gene expression values overlaid onto the IGF-1 Signaling pathway. A) Z score table visualization B) canonical pathway. For A, an orange color indicates a slight upregulation of the pathway and a deeper orange is a strong upregulation of the pathway; a blue color indicates a slight downregulation of the pathway and a deep blue is a strong downregulation of the pathway. A dot in B demonstrates that the result is not statistically significant, where Z is greater than -2 and below 2. A pink color in B indicates slight up-regulation of a gene and a deeper red indicates higher gene expression. A slight green color in B indicates a slight downregulation of the gene and a deep green color indicates high gene downregulation.

In Figure 7, both insulin and $ZnCl_2$ expression values for the genes in this canonical pathway were compared by Ingenuity Pathway Analysis. The researchers have delved into the IGF-1 canonical pathway because it confirms the NGS experiment results that show $ZnCl_2$ is employing the IGF-1 signaling pathway differently than Insulin treated ATDC5 cells. ATDC5 chondrocytes treated with $ZnCl_2$ have a significantly elevated Z score for the IGF-1 signaling pathway than insulin, as shown in A; this is demonstrated by $ZnCl_2$ having a deeper orange color. Therefore, IPA utilizes the gene

expression values from $ZnCl_2$, compares them to the expected gene values from their algorithm and literature database, and produces the canonical pathway results with those values from their analysis. c-fos, c-jun, and grb2 in B are red, meaning that the gene expression values of ATDC5 chondrocytes treated with $ZnCl_2$ are significantly higher in this pathway than the expression values of insulin-treated chondrocytes, as well as being higher than the canonically accepted values. grb10 is green, which indicates a decreased gene expression pattern. grb10 in this pathway leads to the blocking of IGF-R1, marked with a slash through as indicated by the blue arrow.

Canonical Pathway	Insulin (Z score)	Zinc Chloride (Z score)
Superpathway of Inositol Phosphate Compounds	2.116950987	6.337478707
VEGF Family Ligand-Receptor Interactions	2	5.477225575
3-phosphoinositide Biosynthesis	1.459600898	5.897678246
VEGF Signaling	1.941450687	4.706787243
Phospholipase C Signaling	-0.39223227	6.030226892
Osteoarthritis Pathway	0.962250449	4.43760157
GM-CSF Signaling	1.732050808	3.441236008
FGF Signaling	1.212678125	3.528211425
p38 MAPK Signaling	-0.242535625	4.041451884
ERK/MAPK Signaling	0.816496581	3.394673699
NF-κB Signaling	0.19245009	3.904344047
Phospholipases	0.277350098	3.709704134
STAT3 Pathway	-0.534522484	3.429971703
Type II Diabetes Mellitus Signaling	1.697749375	2.2
JAK/Stat Signaling	0.832050294	2.984810029
IGF-1 Signaling	0.632455532	3.152963125
Eicosanoid Signaling	0	3.638034376
Fatty Acid α-oxidation	0.816496581	2.645751311
TGF-β Signaling	0.707106781	2.683281573
Inhibition of Matrix Metalloproteases	-1.414213562	-1.941450687
Fatty Acid Activation	1	2.236067977
Acute Phase Response Signaling	0.208514414	3
Notch Signaling	N/A	1.341640786
Toll-like Receptor Signaling	0	1.264911064
Wnt/β-catenin Signaling	0.447213595	0.169030851
Significance Threshold: -2 ≥ Z ≥ 2		

Table 3: Canonical Pathway output for Insulin and Zinc Chloride treated ATDC5 cells at 24 hours post-treatment. Shown are Z scores of the expression pattern of insulin and zinc chloride treated ATDC5 chondrocytes from IPA's comparison analysis on the gene expression values comparing insulin and $ZnCl_2$. A Z score in this output is a statistical measure of similarity between the expected gene expression relationship direction and the observed gene expression values; scores greater than 2 or below negative 2 are statistically significant in this output. A Z score below negative 2 demonstrates a statistically significant predicted inhibition of that pathway; a Z score above 2 means that there is a statistically significant predicted activation of the pathway.

In this study, NGS data analysis demonstrated that VEGF, GM-CSF, and IGF-1 signaling were significantly differentially regulated when comparing $ZnCl_2$ and insulin treatment groups ($Z_{\text{zinc chloride}} > Z_{\text{insulin}}$). Therefore, our research focused on understanding the importance of VEGF in $ZnCl_2$ mediated chondrogenesis.

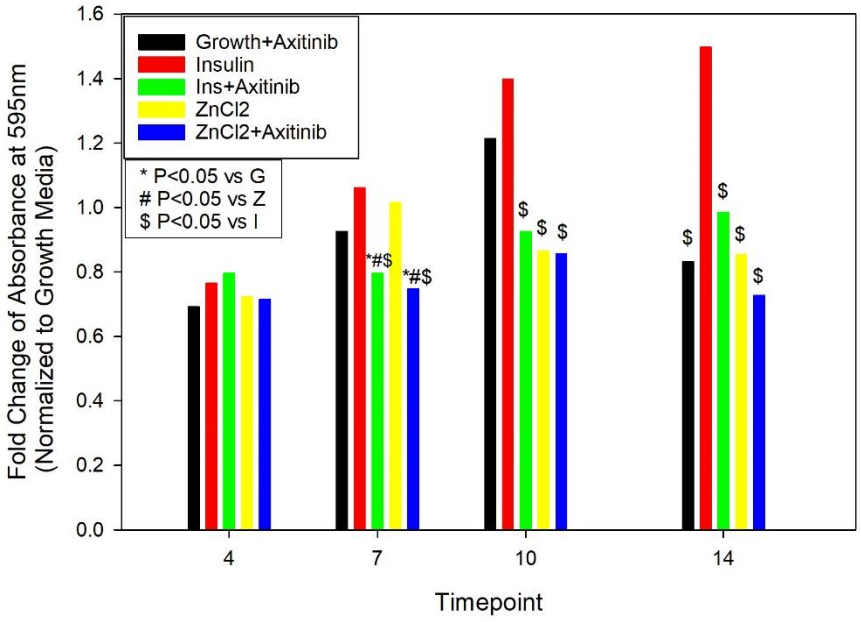

Figure 8: Proteoglycan Deposition Measured in Treated ATDC5 Cells Overtime. Fold changes in absorbance values for each treatment group when normalized to growth media are shown. A fold change below 1 depicts a decreased amount of proteoglycan deposition as compared to growth media, the negative control. A fold change greater than 1 depicts an increase in proteoglycan deposition when compared to the negative control. Statistical significance was determined on the corrected absorbance values of each sample.

At day 7, Axitinib treatment significantly reduced proteoglycan deposition in both $ZnCl_2$ and insulin treated ATDC5 chondrocytes (Figure 8, Table 4). The Insulin+Axitinib and $ZnCl_2$+Axitinib groups were both significantly lower than growth media, insulin, and $ZnCl_2$ in terms of proteoglycan deposition. Insulin+Axitinib's proteoglycan deposition was 20.5% lower than growth media, 25% lower than insulin, and 21.7% lower than $ZnCl_2$ at day 7. $ZnCl_2$ and Axitinib's proteoglycan deposition was 25.3% lower than growth media, 29.6% lower than insulin, and 26.4% lower than $ZnCl_2$ at day 7. On day 10, insulin treatment produced the highest amount of proteoglycan deposition. Insulin was significantly elevated over the Insulin+Axitinib, $ZnCl_2$, and $ZnCl_2$+Axitinib. Insulin

had higher proteoglycan deposition over Insulin+Axitinib by 51.1%, ZnCl2 by 61.8%, and $ZnCl_2$+Axitinib by 63.1%. For day 14, insulin again produced the highest levels of proteoglycan deposition. Insulin's proteoglycan deposition was significantly higher than growth media+Axitinib, Insulin+Axitinib, $ZnCl_2$, and $ZnCl_2$+Axitinib. Insulin was 79.8% elevated over growth media+Axitinib, 51.9% over Insulin+Axitinib, 75.2% over $ZnCl_2$, and 105.6% over $ZnCl_2$+Axitinib. (Figure 8, Table 4)

Day 7				
Comparison	Diff of Me	t	P	P<0.050
Insulin vs ZnCl2+Axitinib	0.028	5.519	0.002	Yes
ZnCl2 vs ZnCl2+Axitinib	0.024	4.73	0.007	Yes
Insulin vs Insulin+Axitinib	0.0237	4.665	0.007	Yes
Growth vs ZnCl2+Axitinib	0.0227	4.468	0.009	Yes
ZnCl2 vs Insulin+Axitinib	0.0197	3.876	0.024	Yes
Growth vs Insulin+Axitinib	0.0183	3.614	0.035	Yes
Day 10				
Comparison	Diff of Me	t	P	P<0.050
Insulin vs ZnCl2+Axitinib	0.0557	4.285	0.016	Yes
Insulin vs ZnCl2	0.055	4.234	0.016	Yes
Insulin vs Insulin+Axitinib	0.0487	3.746	0.036	Yes
Day 14				
Comparison	Diff of Me	t	P	P<0.050
Insulin vs ZnCl2+Axitinib	0.105	6.062	0.002	Yes
Insulin vs ZnCl2	0.0883	5.084	0.007	Yes
Insulin vs Growth+Axitinib	0.0905	4.658	0.012	Yes
Insulin vs Insulin+Axiitnib	0.0703	4.048	0.028	Yes

Table 4: Statistically Significant P-Values of Proteoglycan Deposition Quantitation between groups. This table contains the statistically significant results of the 1-way ANOVA that was ran on the corrected absorbance values of each treatment group. The table shows the timepoint, the treatments being compared, the difference of the means, the t score, the P value, and if the P value is less than 0.05, the statistical significance threshold.

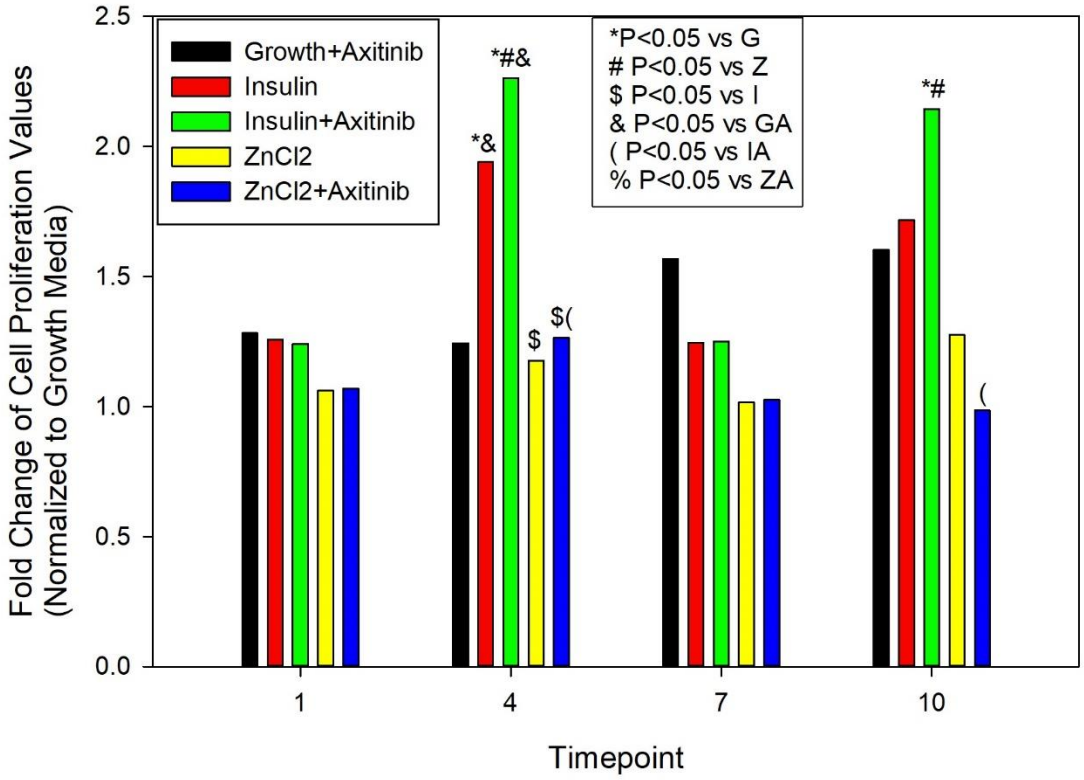

Figure 9: Cell Proliferation Measured through the MTT Assay in Treated ATDC5 Cells. Shown is cellular proliferation value for each treatment group was normalized to growth media to produce fold changes. A fold change below 1 depicts a decreased amount of proteoglycan deposition as compared to growth media, the negative control. A fold change greater than 1 depicts an increase in proteoglycan deposition when compared to the negative control. Statistical significance was determined on the cellular proliferation values of each sample.

At day 4, insulin and Axitinib treated ATDC5 cells have the highest cellular proliferation values of any treatment group (Figure 9, Table 5). Insulin+Axitinib's cellular proliferation is 126% greater than growth media, 92% greater than ZnCl2, and 82% greater than $ZnCl_2$+Axitinib. $ZnCl_2$+Axitinib's cellular proliferation is 34% less than Insulin and 44% less than Insulin+Axitinib. Insulin's cellular proliferation is 94% greater than growth media and 56% greater than growth media and Axitinib. $ZnCl_2$ had 39% less proliferation than insulin. For day 10, the insulin and Axitinib treatment group

once again had the highest cellular proliferation values. $ZnCl_2$+Axitinib had a decreased cellular proliferation of 54% as compared to Insulin+Axitinib. Insulin+Axitinib had increased cellular proliferation over growth media by 114% and 67% greater than $ZnCl_2$.

Day 4				
Comparison	**Diff of Means**	**t**	**P**	**P<0.050**
Insulin+Axitinib vs Growth	126.313	8.944	<0.001	Yes
Insulin+Axitinib vs ZnCl2	108.691	7.697	<0.001	Yes
Insulin+Axitinib vs Growth+Axitinib	101.942	7.219	<0.001	Yes
Insulin+Axitinib vs ZnCl2+Axitinib	99.862	7.071	<0.001	Yes
Insulin vs. Growth	94.037	6.659	<0.001	Yes
Insulin vs. ZnCl2	76.416	5.411	0.002	Yes
Insulin vs. Growth+Axitinib	69.667	4.933	0.003	Yes
Insulin vs. ZnCl2+Axitinib	67.587	4.786	0.004	Yes
Day 10				
Comparison	**Diff of Means**	**t**	**P**	**P<0.050**
Insulin+Axitinibvs. ZnCl2+Axitinib	115.933	5.417	0.002	Yes
Insulin+Axitinib vs. Growth	114.363	5.344	0.002	Yes
Insulin+Axitinib vs. ZnCl2	86.732	4.053	0.021	Yes

Table 5: Statistically Significant P-Values in Cellular Proliferation. This table contains the statistically significant results of the 1-way ANOVA that was ran on the cellular proliferation values of each treatment group in the MTT Assay. The table shows the timepoint, the treatments being compared, the difference of the means, the t score, the P value, and if the P value is less than 0.05, the statistical significance threshold.

Real Time PCR

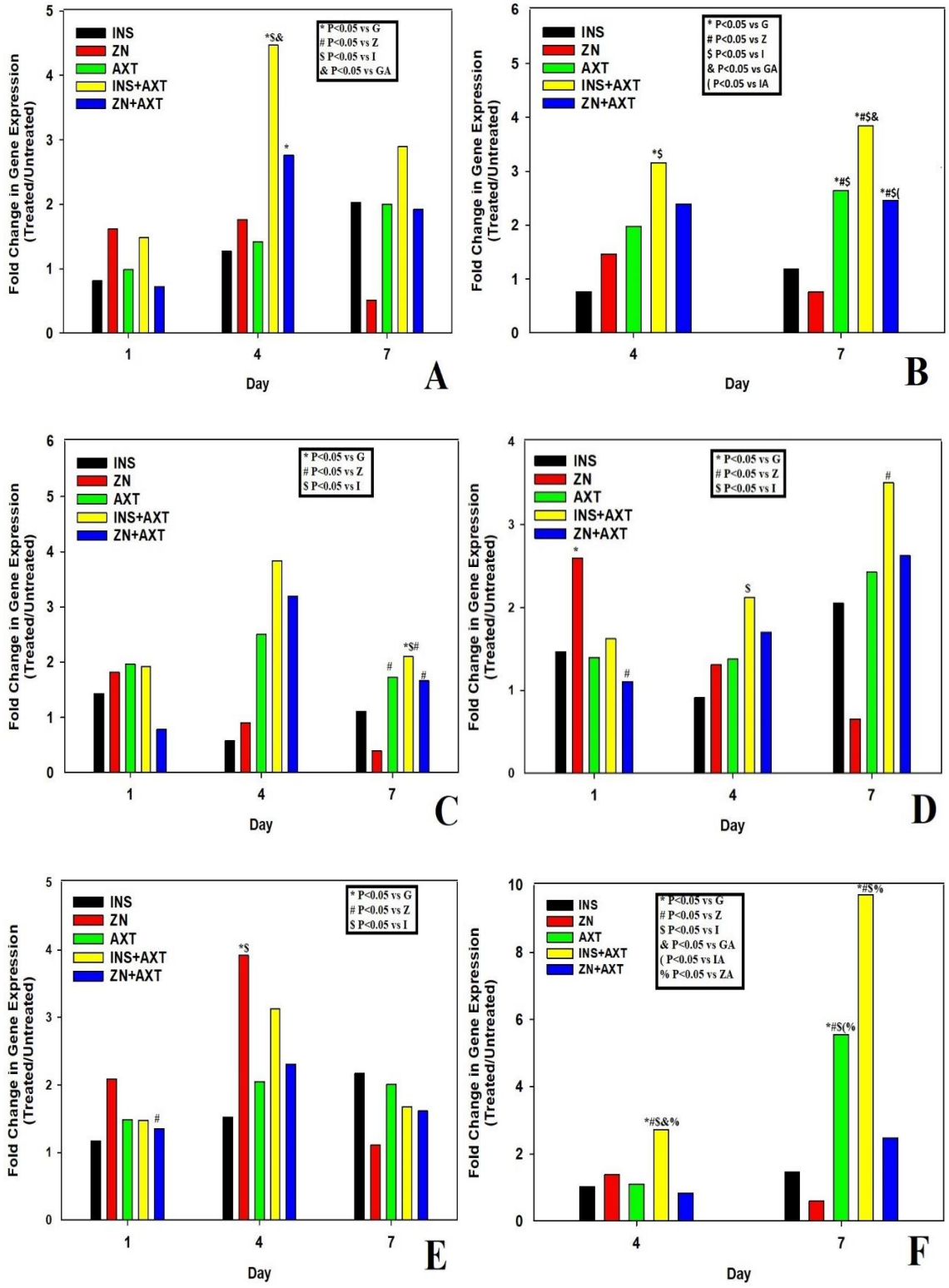

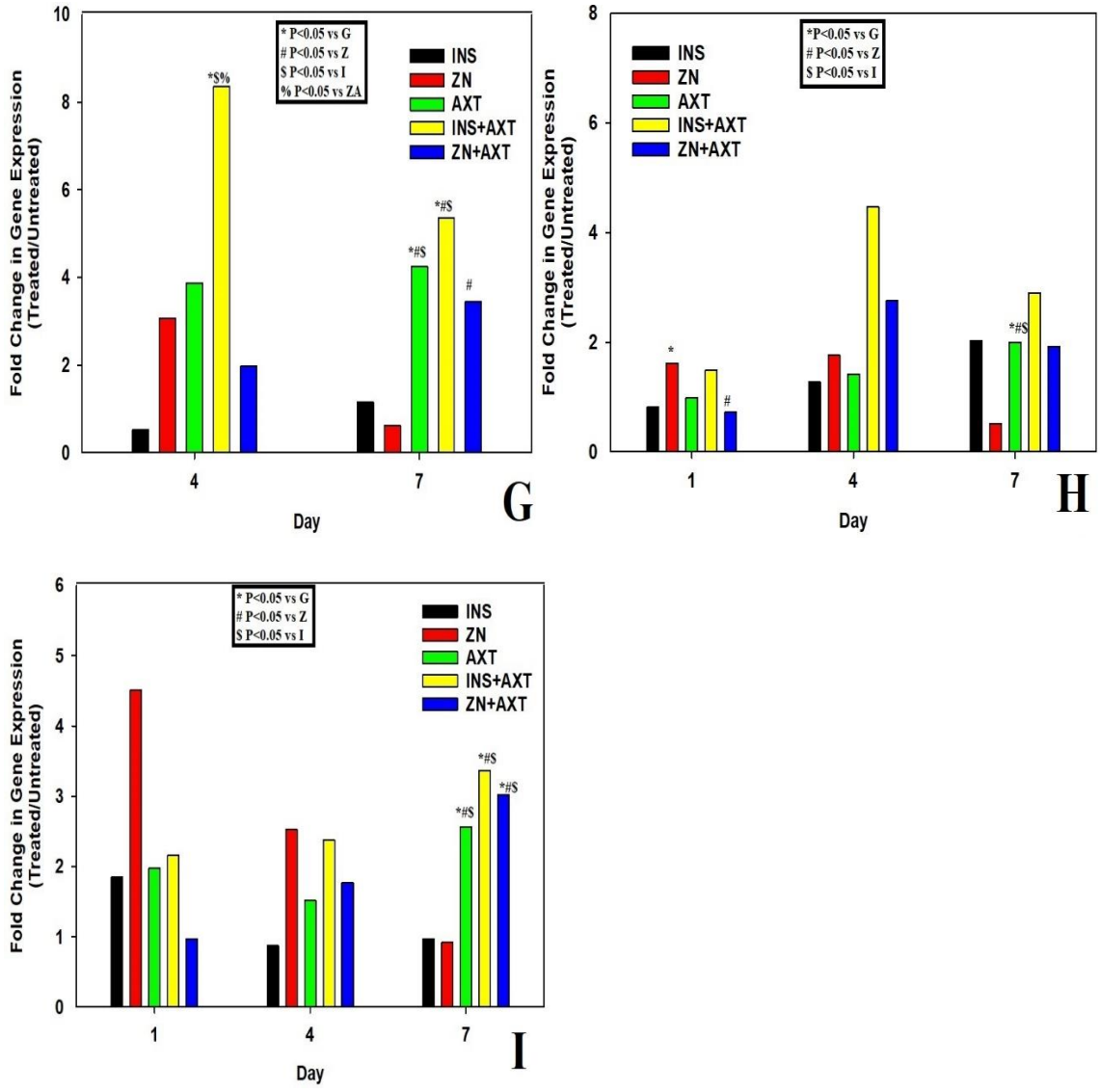

Figure 10: Gene Expression measured with Real-Time Quantitative PCR in Treated ATDC5 Cells. A) VEGFA B) Runx2 C) Jun D) Grb2 E) CycD1 F) Grb10 G) VEGFR2 H) SOX9 I) Runx1. Gene expression cycle threshold (C_T) values were converted to $2^{-\Delta CT}$ values for each treatment group. These $2^{-\Delta CT}$ values were normalized to growth media to produce fold changes. A fold change below 1 depicts a decreased amount of gene expression as compared to growth media, the negative control. A fold change greater than 1 depicts an increase in gene expression when compared to the negative control. Statistical significance was determined on the $2^{-\Delta CT}$ values of each sample.

VEGFA				
Day4				
Comparison	Diff of Means	t	P	P<0.050
AXT + INS D4 vs. CON D4	0.00587	6.781	<0.001	Yes
AXT + INS D4 vs. INS D4	0.00541	6.248	<0.001	Yes
AXT + INS D4 vs. AXT D4	0.00516	5.963	<0.001	Yes
AXT + INS D4 vs. ZN D4	0.00458	5.291	0.002	Yes

Jun				
Day 7				
Comparison	Diff of Means	t	P	P<0.050
AXT+INS D7 vs. ZN D7	0.0105	8.024	<0.001	Yes
AXT D7 vs. ZN D7	0.00823	6.319	<0.001	Yes
AXT + ZN D7 vs. ZN D7	0.00784	6.015	0.001	Yes
AXT+INS D7 vs. CON D7	0.00672	5.161	0.004	Yes
AXT+INS D7 vs. INS D7	0.00606	4.162	0.017	Yes

Runx2				
Day4				
Comparison	Diff of Means	t	P	P<0.050
AXT + INS D4 vs. INS D4	2.007	4.414	0.013	Yes
AXT + INS D4 vs. CON D4	1.81	3.981	0.025	Yes
Day 7				
Comparison	Diff of Means	t	P	P<0.050
AXT+INS D7 vs. ZN D7	2.678	11.037	<0.001	Yes
AXT+INS D7 vs. CON D7	2.468	10.172	<0.001	Yes
AXT+INS D7 vs. INS D7	2.301	8.483	<0.001	Yes
AXT D7 vs. ZN D7	1.636	6.744	<0.001	Yes
AXT + ZN D7 vs. ZN D7	1.479	6.096	<0.001	Yes
AXT D7 vs. CON D7	1.426	5.878	0.001	Yes
AXT + ZN D7 vs. CON D7	1.269	5.23	0.003	Yes
AXT+INS D7 vs. AXT + ZN D7	1.199	4.941	0.004	Yes
AXT D7 vs. INS D7	1.259	4.643	0.005	Yes
AXT+INS D7 vs. AXT D7	1.042	4.294	0.008	Yes
AXT + ZN D7 vs. INS D7	1.102	4.063	0.009	Yes

CycD1				
Day 1				
Comparison	Diff of Means	t	P	P<0.050
ZN D1 vs. AXT+Zn D1	1.795	4.706	0.032	Yes
Day 4				
Comparison	Diff of Means	t	P	P<0.050
ZN D4 vs. CON D4	0.0239	4.675	0.008	Yes
ZN D4 vs. INS D4	0.0196	3.834	0.033	Yes

Grb2				
Day 1				
Comparison	Diff of Means	t	P	P<0.050
ZN D1 vs. CON D1	0.98	5.078	0.034	Yes
ZN D1 vs. AXT+Zn D1	0.915	4.745	0.044	Yes
Day 4				
Comparison	Diff of Means	t	P	P<0.050
AXT + INS D4 vs. INS D4	0.0298	3.707	0.044	Yes
Day 7				
Comparison	Diff of Means	t	P	P<0.050
AXT+INS D7 vs. ZN D7	0.0628	3.719	0.043	Yes

VEGFR2				
Day 4				
Comparison	Diff of Means	t	P	P<0.050
AXT + INS D4 vs. INS D4	0.000313	4.437	0.012	Yes
AXT + INS D4 vs. CON D4	0.000294	4.168	0.018	Yes
AXT + INS D4 vs. AXT + ZN D4	0.000255	3.617	0.045	Yes
Day 7				
Comparison	Diff of Means	t	P	P<0.050
AXT+INS D7 vs. ZN D7	0.000453	5.852	0.001	Yes
AXT+INS D7 vs. CON D7	0.000417	5.382	0.002	Yes
AXT+INS D7 vs. INS D7	0.000401	5.181	0.003	Yes
AXT D7 vs. ZN D7	0.000346	4.475	0.009	Yes
AXT D7 vs. CON D7	0.00031	4.005	0.019	Yes
AXT D7 vs. INS D7	0.000294	3.804	0.025	Yes
AXT + ZN D7 vs. ZN D7	0.000271	3.495	0.039	Yes

Grb10				
Day 4				
Comparison	Diff of Means	t	P	P<0.050
AXT + INS D4 vs. AXT + ZN D4	0.000535	5.503	0.002	Yes
AXT + INS D4 vs. CON D4	0.000487	5.012	0.004	Yes
AXT + INS D4 vs. INS D4	0.000479	4.931	0.005	Yes
AXT + INS D4 vs. AXT D4	0.00046	4.735	0.006	Yes
AXT + INS D4 vs. ZN D4	0.000379	3.899	0.023	Yes
Day 7				
Comparison	Diff of Means	t	P	P<0.050
IA 7d vs. Z 7d	0.00129	15.108	<0.001	Yes
IA 7d vs. G 7d	0.00124	14.448	<0.001	Yes
IA 7d vs. I 7d	0.00117	13.693	<0.001	Yes
IA 7d vs. ZA 7d	0.00103	11.997	<0.001	Yes
GA 7d vs. Z 7d	0.000703	8.217	<0.001	Yes
GA 7d vs. G 7d	0.000647	7.556	<0.001	Yes
IA 7d vs. GA 7d	0.00059	6.892	<0.001	Yes
GA 7d vs. I 7d	0.000582	6.801	<0.001	Yes
GA 7d vs. ZA 7d	0.000437	5.106	0.002	Yes

SOX9				
Day 1				
Comparison	Diff of Means	t	P	P<0.050
ZN D1 vs. AXT+Zn D1	10.542	5.217	0.012	Yes
ZN D1 vs. CON D1	8.45	4.182	0.042	Yes
Day 7				
Comparison	Diff of Means	t	P	P<0.050
AXT D7 vs. INS D7	0.0186	4.185	0.019	Yes
AXT D7 vs. ZN D7	0.0184	4.141	0.019	Yes
AXT D7 vs. CON D7	0.0174	3.926	0.026	Yes

Runx1				
Day 7				
Comparison	Diff of Means	t	P	P<0.050
AXT+INS D7 vs. CON D7	0.0414	8.084	<0.001	Yes
AXT+INS D7 vs. ZN D7	0.0428	7.476	<0.001	Yes
AXT+INS D7 vs. INS D7	0.0419	7.312	<0.001	Yes
AXT + ZN D7 vs. CON D7	0.0353	6.902	<0.001	Yes
AXT + ZN D7 vs. ZN D7	0.0367	6.419	<0.001	Yes
AXT + ZN D7 vs. INS D7	0.0358	6.255	<0.001	Yes
AXT D7 vs. CON D7	0.0274	5.348	0.003	Yes
AXT D7 vs. ZN D7	0.0288	5.029	0.004	Yes
AXT D7 vs. INS D7	0.0278	4.865	0.005	Yes

Table 6: Statistically Significant P Values from Real Time Quantitative PCR Experiment. This table contains the statistically significant results of the 1-way ANOVA that was ran on the corrected absorbance values of each treatment group in the Real Time Quantitative PCR Experiment. The table shows the timepoint, the treatments being compared, the difference of the means, the t score, the P value, and if the P value is less than 0.05, the statistical significance threshold.

VEGFA expression at the 4-day timepoint demonstrated that Insulin+Axitinib was 374.3% elevated over growth media, 251.6% increased as compared to insulin, and 215% above Growth+Axitinib. $ZnCl_2$+Axitinib- treated VEGFA gene expression was 176.3% above growth media at the same timepoint. Gene expression of the runx2 gene at 4 days was significantly upregulated in Insulin+Axitinib treated ATDC5 cells by 313.1% over insulin and 216% over growth media. Runx2 at 7 days had more treatment groups have statistically different gene expression values. Growth+Axitinib was 164.6% increased over growth media, 249.2% over $ZnCl_2$, and 121.9% above insulin. $ZnCl_2$+Axitnib had gene expression 146.4% above growth media, 106.6% over insulin, 225.1% over $ZnCl_2$, and 36% below Insulin+Axitinib. Insulin+Axitinib- treated gene expression was increased by 284.7% over growth media, 407.6% over $ZnCl_2$, 222.5% over insulin, and 45.4% over Growth+Axitinib.

Jun gene expression in treated ATDC5 chondrocytes only had statistically significant differential gene expression at the 7-day timepoint. Insulin+Axitinib at this timepoint had gene expression 90% over insulin, 110.4% over growth media, and 437.5% over $ZnCl_2$. Growth+Axitinib gene expression was 341.7% increased above $ZnCl_2$; jun gene expression in $ZnCl_2$+Axitinib-treated chondrocytes was 325% above $ZnCl_2$. Grb2's gene expression values at day 1 demonstrated that $ZnCl_2$ treatment increased grb2 expression by 135% over $ZnCl_2$+Axitinib and 159.3% over growth. At 4 days, the only statistically significant differential gene expression in grb2 was Insulin+Axitinib being 133% over insulin. Statistically significant differential gene expression for grb2 at 7 days had solely $ZnCl_2$ being 81.3% below Insulin+Axitinib.

Cyclin D1 gene expression at day 1 only yielded one statistically significant result: $ZnCl_2$ was elevated over $ZnCl_2$+Axitinib by 140.3%. For day 4, $ZnCl_2$-treated cycD1 gene expression was 292.4% above growth media and 156.8% over insulin. Grb10 gene expression at 4 days yielded results that Insulin+Axitinib expression for this gene is 172.1% elevated over growth media, 164.6% over insulin, 148.4% over Growth+Axitinib, and 96.9% over $ZnCl_2$. $ZnCl_2$+Axitinib gene expression for grb10 at 4 days is 69.5% below Insulin+Axitinib. At 7 days, grb10 gene expression had numerous statistically significant differential gene expressions. Insulin+Axitinib was elevated by 567% over insulin, 872% over growth media, 74.9% over Growth+Axitinib, and 1508% over $ZnCl_2$. For the same timepoint, Growth+Axitinib was 281% above insulin, 456% above growth media, and 820% above $ZnCl_2$; $ZnCl_2$+Axitinib gene expression for grb10

at 7 days was 55.4% lower than Growth+Axitinib and 74.5% lower than Insulin+Axitinib.

Vegfr2 expression at the 4-day timepoint, when treated with Insulin+Axitinib, is 1490% elevated over insulin and 735% over growth media. $ZnCl_2$+Axitinib- treated Vegfr2 expression at this timepoint is decreased by 76.4% when compared to Insulin+Axitinib. At 7 days, Insulin+Axitinib Vegfr2 gene expression is 768% over $ZnCl_2$, 437% over growth media, and 361% over insulin. Growth+Axitinib- treated gene expression for Vegfr2 at 7 days is 586% above $ZnCl_2$, 325% above growth media, and 265% above insulin; $ZnCl_2$ expression is 82.1% below $ZnCl_2$+Axitinib.

$ZnCl_2$+Axitinib- treated expression of SOX9 at 1 day is 69% below $ZnCl_2$; $ZnCl_2$ expression is 124% above growth media. At 7 days, Growth+Axitinib treated ATDC5 chondrocytes' gene expression is elevated by 747% over insulin, 684% over $ZnCl_2$, and 480% over growth media. Runx1 gene expression in the qPCR experiment only yielded statistically significant differential gene expression at the 7-day timepoint. Insulin+Axitinib is elevated by 237% over growth media, 266% over $ZnCl_2$, and 246% over insulin. Growth+Axitinib is higher than growth media by 157%, $ZnCl_2$ by 179%, and insulin by 164%. $ZnCl_2$+Axitinib expression for runx1 at 7 days is above $ZnCl_2$ by 228%, growth by 202%, and insulin by 211%.

Discussion

Bone fracture healing is a diverse field that often focuses on biological research that aims to improve or understand bone fracture healing. More specifically, a facet of this field focuses on improving patient healing outcomes for patients with diabetes that impair normal bone healing. As a result, a substantial literature exists which describes the role of insulin in both diabetic and normal healing. Studies such as Gandhi et. al (2005) and Graves et. al (2011) have demonstrated using a diabetic fracture model that insulin is necessary for proper bone healing. When non-diabetic or diabetic animals are provided insulin at the fracture site, bone healing is improved (Cornish et. al, 1996). Unfortunately, providing insulin to patients is problematic because insulin plays a major role on regulating sugar levels; therefore, giving a patient insulin can affect sugar levels causing side effects including swelling, weight gain, dizziness, moodiness, seizures, and death. Therefore, some researchers have begun investigating whether insulin mimetics such as $ZnCl_2$ could promote bone healing in both non-diabetic and diabetic fracture healing similarly to insulin. In fact, research has shown that treatment with $ZnCl_2$ in a non-diabetic (Wey et. al, 2014) and diabetic (Bortolin et. al, 2015) rodent fracture model accelerate bone healing. Although, these positive results are promising, the mechanism by which these insulin mimetics is not well understood. A better understanding of this mechanism will be important to provide the best possible therapeutics for diabetic patients. Our research focused on understanding the mechanism by which $ZnCl_2$ affects chondrogenesis, an important component of bone fracture healing.

Next Generation Sequencing showed that VEGFA and VEGFB gene expression levels were consistent between both insulin and $ZnCl_2$; however, only $ZnCl_2$ treated chondrocytes utilized flt1, the VEGFR1 receptor. This was further corroborated by Ingenuity Pathway Analysis' comparison analysis and canonical pathway analysis, which demonstrated that VEGFR2 was significantly upregulated in $ZnCl_2$ treated chondrocytes when compared to insulin. IPA also demonstrated that the downstream regulators of VEGFA & C and VEGFR1&2, Grb2 and c-Fos, were significantly elevated in $ZnCl_2$ treated chondrocytes when compared to insulin. The NGS data also showed that jun and junb were both significantly increased in both insulin and $ZnCl_2$ treated chondrocytes, but only jund was exclusively utilized by $ZnCl_2$ treated chondrocytes. Due to increased levels of grb2 in $ZnCl_2$ treated ATDC5 cells, the data suggests that the Akt pathway may be important to this mechanism. Burgess et. al demonstrated similar data in ATDC5 cells that showed that $ZnCl_2$ could lead to the upregulation of mTOR, an important factor in the Akt pathway (Burgess et. al, 2017). Mukherjee and Rotwein have also shown that Akt is crucial to bone healing using a histological sectioning method of mouse metatarsal bones that were incubated ex vivo; their results show that inhibition of Akt activity leads to impaired cartilage grown and impairments in osteoblast function and development (Mukherjee and Rotwein, 2009).

The NGS data shows that $ZnCl_2$ and insulin can also signal through overlapping pathways. We demonstrated with NGS that runx3 was upregulated equally by both insulin and $ZnCl_2$, but neither had any statistically significant difference when compared to the other. In the qPCR data, runx2 at 4-day and 7-day timepoints had no significant

difference between insulin and $ZnCl_2$ treatment when compared to growth media. Runx2 has been shown to regulate the gene network that is associated with insulin signaling (Adhami et. al, 2011). Runx2 has also been demonstrated to accelerate fracture healing in ZnCl2 (Wey et. al, 2014; Liu et. al, 2012).

When analyzing the effects of insulin and $ZnCl_2$ on IGF-1 signaling canonical pathway, insulin did not have a statistically significant Z score. However, $ZnCl_2$ did significantly elevate IGF-1 signaling. Zinc has been shown to signal through the insulin pathway as both insulin and zinc were able to independently lead to the phosphorylation of p38, GSK-3B, ERK1/2, Akt, and glucose oxidation (Norouzi et. al, 2018). Vanadium sulfate has been shown to induce normoglycemia, prevent pancreatic islet atrophy, and proliferate pancreatic beta cells as well as induce antilipolytic effects through Akt activation, demonstrating its effects as an insulin mimetic (Pirmoradi et. al, 2016; Liu et. al, 2013). Burgess has also demonstrated that ZnCl2 activated Akt as a component of its insulin mimetic mechanisms (Burgess and Cottrell, 2017). On the other hand, this demonstrates results that confirm the previous literature that $ZnCl_2$ is an insulin mimetic, as it is utilizing this pathway. Additionally, c-jun and c-fos downstream regulators of the IGF-1 pathway are also elevated by $ZnCl_2$ treated chondrocytes only. Induction of the IGF-1 (Laron, 2001) and VEGF (Hu et. al, 2016) pathways has previously been shown to increase cell proliferation and growth. As a result, the increases in proteoglycan deposition and cell proliferation seen in our data may be a result of $ZnCl_2$ induction of the IGF-1 pathway. Burgess also demonstrated statistically significant increase in

proteoglycan deposition in 100uM $ZnCl_2$ treated ATDC5 cells at the 14 and 17-day timepoints (Burgess and Cottrell, 2017).

When the VEGF pathway was inhibited in $ZnCl_2$- or insulin-treated cells significant decreases in proteoglycan deposition occurred on day 7 and 14 (P=0.007 for $ZnCl_2$, P=0.028 for insulin) when compared to controls. VEGF is known to be important to vasculature development which is important for bone repair and chondrogenesis. Mice with VEGF deficient osteoblast precursor cells cause an osteoporosis-like phenotype with reduced bone mass and reduced osteoblast differentiation (Liu et. al, 2012). In a Sprague-Dawley rat model where they received the VEGF inhibitor TNP-470, their unilateral closed femoral fractures resulted in non-unions; this was due to the lack of vasculature caused by the lack of VEGF due to the inhibitor; the rats that did not have inhibition did not suffer adverse healing of their fracture (Keramaris et. al, 2008).

Our data demonstrates that at later timepoints, VEGF inhibition produces higher amounts of genes such as jun, grb2, and cyclin D1 which were identified in the NGS data and confirmed through QPCR. These mediators are all crucial for cell cycle progression, cell proliferation, and cell growth. Jun and other AP-1 members have been demonstrated to increase chondrocytes to become hypertrophic through contributing to Sox9's actions (He et. al, 2016). Cyclin D1, as stimulated by TGF-β, aids in chondrocyte maturation and proliferation (Li et. al, 2006); our results from the NGS experiment demonstrate an increase in the TGF- β family as well.

Our data also demonstrated that $ZnCl_2$ significantly increases the expression of various collagen genes as well as BMP6. These genes are crucial for cartilage matrix

formation and bone formation. Collagen 17a1 is a component of epithelial and mesenchymal interactions, two types of tissue that rely on matrix interactions. Col17a1 deficiency, as demonstrated through a collage 17 knock out mouse model and a collagen 17 rescue model, causes diminished levels of iron deposition, delayed calcification, and enamel hypoplasia (Asaka et. al, 2009). BMP6 is a growth factor that has been shown to enhance chondrogenesis in marrow stromal cells; the cells being treated with BMP also had higher proteoglycan staining results (Sekiya et. al, 2001), as seen in this research. We believe that $ZnCl_2$ upregulating many members of the collagen family and BMP6, which insulin is not, is a component of its success as an insulin mimetic in bone healing.

Runx1 is not usually thought of as a key mediator in bone healing. Most research demonstrates that runx2 is essential for bone development. However, in the NGS experiment, only $ZnCl_2$ chondrocytes upregulated the runx1 gene not runx2. Burgess also found that there were no significant differences in runx2 expression when comparing treatment groups over time (Burgess and Cottrell, 2017). However, our qPCR gene expression data showed that runx2 had decreased expression in chondrocytes treated with $ZnCl_2$ and VEGF inhibitor when compared to $ZnCl_2$ alone. However, runx1 was significantly elevated in $ZnCl_2$+VEGF inhibitor as compared to $ZnCl_2$ alone. This data suggests that in the presence of a VEGF that runx1 may be an important mediator in $ZnCl_2$- mediated chondrogenesis.

Conclusions

Bone formation can be aided by both $ZnCl_2$ treatment and insulin treatment. Although the mechanisms by which $ZnCl_2$ and insulin have been shown to overlap, our data suggests that $ZnCl_2$ works through a mechanism different then insulin when employing the VEGF- pathway. Future studies could include quantifying protein expression to determine if these gene expression patterns are similar at the protein level.

References

Adhami, M., Ghori-Javed, F. Y., Chen, H., Gutierrez, S. E., & Javed, A. (2011). Runx2 regulates the gene network associated with insulin signaling and energy homeostasis. *Cells, tissues, organs*, *194*(2-4), 232–237. doi:10.1159/000324763

Ai-Aql ZS, Alagl AS, Graves DT, Gerstenfeld LC, Einhorn TA. Molecular mechanisms controlling bone formation during fracture healing and distraction osteogenesis. Journal of Dental Research. 2008;87(2):107–18.

American Diabetes Association. Statistics About Diabetes. 2018, March 22. http://www.diabetes.org/diabetes-basics/statistics/

Asaka, T., Akiyama, M., Domon, T., Nishie, W., Natsuga, K., Fujita, Y., Abe, R., Kitagawa, Y., Shimizu, H. (2009). Type XVII collagen is a key player in tooth enamel formation. *The American journal of pathology*, *174*(1), 91–100. doi:10.2353/ajpath.2009.080573

Bais MV, Wigner N, Young M, Toholka R, Graves DT, Morgan EF, Gerstenfeld LC, Einhorn TA. BMP2 is essential for post-natal osteogenesis but not for recruitment of osteogenic stem cells. Bone. 2009;45(2):254–66.

Becker A and Roth R. Insulin receptor structure and function in normal and pathological conditions. Annual Review of Medicine. 1990; 41:99-115. doi.org/10.1146/annurev.me.41.020190.000531

Berendsen A and Olsen B (2014). How vascular endothelial growth factor-A (VEGF) regulates differentiation of mesenchymal stem cells. Journal of Histochemistry & Cytochemistry, 62(2) 103-108.

Beyersmann D and Haase H. Functions of zinc in signaling, proliferation and differentiation of mammalian cells. BioMetals. 2001; 14:331-341

Bilezikian J, Raisz, L, and Rodan G. (2002). *Principles of Bone Biology*. San Diego, California: Academic Press.

Bortolin RH, da Graca Azevedo Abreu BJ, Abbott Galvao Uruahy M, Costa de Souza KS, Bezerra JF, Loureiro MB, da Silva FS, Marques DE, Batista AA, Oliveira G, Luchessi AD, Lima VM, Miranda CE, Lia Fook MV, Almeida Md, de Rezende LA, de Rezende AA. (2015). Protection against T1DM-Induced Bone Loss by Zinc Supplementation: Biomechanical, Histomorphometric, and Molecular Analyses in STZ-Induced Diabetic Rats. *PloS one*, *10*(5), e0125349. doi:10.1371/journal.pone.0125349

Bravo D, Gleason J, Sanchez R, Roth R, and Fuller R. Accurate and efficient cleavage of the human insulin proreceptor by the human proprotein-processing protease furin. Characterization and kinetic parameters using the purified, secreted soluble protease expressed by a recombinant baculovirus. Journal of Biological Chemistry. 1994; 269(41):25830-7

Bruder S P, Caplan A I . Cellular and molecular events during embryonic bone development. Connect. Tissue Res. 1989;20:65–71.

Burgess D and Cottrell J. Zinc chloride activates phospho-AKT and promotes chondrocyte maturation in the ATDC5 chondrogenic cell line. Seton Hall University Dissertations and Theses (ETDS). 2017. Retrieved from:

https://scholarship.shu.edu/dissertations/2446/?utm_source=scholarship.shu.edu%2Fdissertations%2F2446&utm_medium=PDF&utm_campaign=PDFCoverPages

Carmeliet P, Collen D (1999). Role of vascular endothelial growth factor and vascular endothelial growth factor receptors in vascular development. Curr Top Microbiol Immunol 237:133-158.

Carlevaro M, Cermelli S, Cancedda R, and Descalzi Cancedda F. Vascular endothelial growth factor (VEGF) in cartilage neovascularization and chondrocyte differentiation: auto-paracrine role during endochondral bone formation. *Journal of Cell Science*. 2000; 113,59-69. http://jcs.biologists.org/content/113/1/59.long

Chen H, Ghori-Javed F, Rashid H, Adhami M, Serra R, Gutierrez S, and Javed A. Runx2 regulates endochondral ossification through control of chondrocyte proliferation and differentiation. Journal of Bone Mineral Research. 2014; 29(12):2653-2665. doi:10.1002/jbmr.2287

Chen Y, Alman BA. Wnt pathway, an essential role in bone regeneration. Journal of Cellular Biochemistry. 2009;106(3):353–62.

Cho TJ, Gerstenfeld LC, Einhorn TA. Differential temporal expression of members of the transforming growth factor beta superfamily during murine fracture healing. Journal of Bone & Mineral Research. 2002;17(3):513–20.

Cho HH, Kyoung KM, Seo MJ, Kim YJ, Bae YC, Jung JS. Overexpression of CXCR4 increases migration and proliferation of human adipose tissue stromal cells. Stem Cells & Development. 2006;15(6):853–64.

Cornish J, Callon K, and Reid I. Insulin increases histomorphometric indices of bone formation in vivo. Calcified Tissue Internation. 1996; 59(6): 492-495. doi:10.1007/s002239900163.

Cserjesi P, Brown D, Ligon KL, Lyons GE, Copeland NG, Gilbert DJ, Jenkins NA, Olson EN. Scleraxis: a basic helix-loop-helix protein that prefigures skeletal formation during mouse embryogenesis. Development, 1995; 121: 1099-1110.

Deckers MM, van Bezooijen RL, van der Horst G, Hoogendam J, van Der Bent C, Papapoulos SE, Lowik CW. Bone morphogenetic proteins stimulate angiogenesis through osteoblast-derived vascular endothelial growth factor A. Endocrinology. 2002;143:1545–1553.

Dedania J, Borzio R, Paglia D, Breitbart EA, Mitchell A, Vaidya S, Wey A, Mehta S, Benevenia J, O'Connor JP, Lin SS. 2011. Role of local insulin augmentation upon allograft incorporation in a rat femoral defect model. Journal of Orthopaedic Research. 29(1); 92-99. doi:10.1002/jor.21205

Fantl W, Johnson D, and Williams L. Signalling by receptor tyrosine kinases. Annual Review of Biochemistry. 1993; 62:453-481 doi.org/10.1146/annurev.bi.62.070193.002321

Feldser D, Agani F, Iyer NV, Pak B, Ferreira G, Semenza GL: Reciprocal positive regulation of hypoxia-inducible factor 1alpha and insulin-like growth factor 2. Cancer Res, 1999; 59: 3915-18.

Gandhi A, Beam H, O'Connor J, Parsons R, and Lin S. The effects of local insulin delivery on diabetic fracture healing. *Bone*. 2005; 37(4), 482-90. https://doi.org/10.1016/j.bone.2005.04.039

Gerstenfeld LC, Cullinane DM, Barnes GL, Graves DT, Einhorn TA. Fracture healing as a post-natal developmental process: molecular, spatial, and temporal aspects of its regulation. Journal of Cellular Biochemistry. 2003;88(5):873–84.

Gilbert SF. Developmental Biology. 6th edition. Sunderland (MA): Sinauer Associates; 2000. Osteogenesis: The Development of Bones. Available from: https://www.ncbi.nlm.nih.gov/books/NBK10056/

Goldring MB, Tsuchimochi K, and Ijiri K. The control of chondrogenesis. Journal of Cellular Biochemistry. 2006; 97:33-44.

Granero-Molto F, Weis JA, Miga MI, Landis B, Myers TJ, O'Rear L, Longobardi L, Jansen ED, Mortlock DP, Spagnoli A. Regenerative effects of transplanted mesenchymal stem cells in fracture healing. Stem Cells. 2009;27(8):1887–98.

Graves, D. T., Alblowi, J., Paglia, D. N., O'Connor, J. P., & Lin, S. (2011). Impact of Diabetes on Fracture Healing. Journal of Experimental & Clinical Medicine, 3(1), 3-8. doi:10.1016/j.jecm.2010.12.006

He, X., Ohba, S., Hojo, H., & McMahon, A. P. (2016). AP-1 family members act with Sox9 to promote chondrocyte hypertrophy. *Development (Cambridge, England)*, *143*(16), 3012–3023. doi:10.1242/dev.134502

Hoeppner LH, Sinha S, Wang Y, Bhattacharya R, Dutta S, Gong X, Bedell VM, Suresh S, Chun C, Ramchandran R, Ekker SC, Mukhopadhyay D. RhoC maintains

vascular homeostasis by regulating VEGF-induced signaling in endothelial cells. J Cell Sci. 2015; 128:3556-3568.

Howell S, Young D, and Lacy P. Isolation and properties of secretory granules from rat islets of Langerhans. Journal of Cell Biology. 1969; 41(1),167-176. doi:10.1083/jcb.41.1.167

Hrynyk, M., & Neufeld, R. J. (2014). Insulin and wound healing. Burns, 40(8), 1433-1446. doi:10.1016/j.burns.2014.03.020

Hu K, Olsen BR. Osteoblast-derived VEGF regulates osteoblast differentiation and bone formation during bone repair. J Clin Invest. 2016; 126:509–526. [PubMed: 26731472]

Hu K and Olsen B. The roles of vascular endothelial growth factor in bone repair and regeneration. *Bone*. 2016 October; 91:30-38. doi:10/1016/j.bone.2016.06.013

Igarashi A and Yamaguchi M. Increase in bone growth factors with healing rat fractures: the enhancing effect of zinc. *International Journal of Molecular Medicine*. 2001; 8(4): 433-438. doi.org/10.3892/ijmm.8.4.433

Iwata K, Asawa Y, Fujihara Y, Tanaka Y, Nishizawa S, Nakagawa T, Nagata S, Takato T, Hoshi K. The effects of rapid- or intermediate-acting insulin on the proliferation and differentiation of cultured chondrocytes. Current Aging Science. 2010; 3(1): 26-33. doi:10.2174/1874609811003010026

Jiao, H., Xiao, E., & Graves, D. T. (2015). Diabetes and Its Effect on Bone and Fracture Healing. *Current osteoporosis reports*, *13*(5), 327–335. doi:10.1007/s11914-015-0286-8

Joyce M, Roberts A, Sporn M, and Bolander M. Transforming Growth Factor-B and the initiation of chondrogenesis and osteogenesis in the rat femur. Journal of Cell Biology. 1990; 110:2195-2207.

Kaji T, Fujiwara Y, Yamamoto C, Sakamoto M, and Kozuka H. Stimulation by zinc of cultured vascular endothelial cell proliferation: Possible involvement of endogenous basic fibroblast growth factor. *Life Sciences*. 1994; 55(23), 1781-87.

Keramaris NC, Calori GM, Nikolaou VS, Schemitsch EH, Giannoudis PV. Fracture vascularity and bone healing: a systematic review of the role of VEGF. Injury. 2008;39(Suppl 2):S45–57.

Kitaori T, Ito H, Schwarz EM, Tsutsumi R, Yoshitomi H, Oishi S, Nakano M, Fujii N, Nagasawa T, Nakamura T. Stromal cell-derived factor 1/CXCR4 signaling is critical for the recruitment of mesenchymal stem cells to the fracture site during skeletal repair in a mouse model. Arthritis & Rheumatism. 2009;60(3):813–23.

Koerner J, Vives M, O'Connor P, Chirichella P, Breitbart E, Chaudhary S, Uko L, Subramanian S, Fritton K, Benevenia K, and Lin S. Zinc has insulin-mimetic properties which enhance spinal fusion in a rat model. The Spine Journal. 2016; 16(6):777-783. http://dx.doi.org/10.1016/j.spinee.2016.01.190.

Komori T, Yagi H, Nomura S, Yamaguchi A, Sasaki K, Deguchi K, Shimizu Y, Bronson R, Gao Y, Inada M, Sato M, Okamoto R, Kitamura Y, Yoshiki S, Kishimoto T. *Cell*. Targeted disruption of Cbfa1 results in a complete lack of bone formation owing to maturational arrest of osteoblasts. 1997; 89(5), 755-64.

Kon T, Cho TJ, Aizawa T, Yamazaki M, Nooh N, Graves D, Gerstenfeld LC, Einhorn TA. Expression of osteoprotegerin, receptor activator of NF-kappaB ligand (osteoprotegerin ligand) and related proinflammatory cytokines during fracture healing. Journal of Bone & Mineral Research. 2001;16(6):1004–14.

Krell E, Ippolito J, Montemurro N, Lim P, Vincent R, Hreha H, Cottrell J, Sudah S, Munoz M, Pacific K, Benevenia J, O'Connor J, and Lin S. Local zinc chloride release from a calcium sulfate carrier enhances fracture healing. *Journal of Orthopaedic Trauma*. 2017; 31(3), 168-174. DOI: 10.1097/BOT.0000000000000748

Laron Z. (2001). Insulin-like growth factor 1 (IGF-1): a growth hormone. *Molecular pathology : MP*, *54*(5), 311–316. doi:10.1136/mp.54.5.311

Lee J and Pilch P. The insulin receptor: structure, function, and signaling. American Journal of Physiology. 1994; 266(2): C319-C334.

Liao J, Hu N, Zhou N, Lin L, Zhao C, Yi S, Fan T, Bao W, Liang X, Chen H, Xu W, Chen C, Cheng Q, Zeng Y, Si W, Yang Z, and Huang W. Sox9 potentiates BMP-2 induced chondrogenic differentiation and inhibits BMP-2 induced osteogenic differentiation. PLoS ONE 9(2): e89025. doi:10.1371/journal.pone.0089025

Li TF, Chen D, Wu Q, Chen M, Sheu TJ, Schwarz EM, Drissi H, Zuscik M, O'Keefe RJ. Transforming growth factor-beta stimulates cyclin D1 expression through activation of beta-catenin signaling in chondrocytes. *J Biol Chem*. 2006 Jul 28;281(30):21296-304. doi: 10.1074/jbc.M600514200. Epub 2006 May 10. PubMed PMID: 16690606; PubMed Central PMCID: PMC2649822.

Lima M, Caricilli A, de Abreu L, Araujo E, Pelegrinelli F, Thirone A, Tsukumo D, Pessoa A, dos Santos M, de Moraes M, Carvalheira J, Velloso L, and Saad M. Topical insulin accelerates wound healing in diabetes by enhancing the AKT and ERK pathways: a double-blind placebo-controlled clinical trial. PLoS ONE 7(5): e36974. 2012. https://doi.org/10.1371/journal.pone.0036974

Liu, Y., Berendsen, A. D., Jia, S., Lotinun, S., Baron, R., Ferrara, N., & Olsen, B. R. (2012). Intracellular VEGF regulates the balance between osteoblast and adipocyte differentiation. *The Journal of clinical investigation*, *122*(9), 3101–3113. doi:10.1172/JCI61209

Liu JC, yu Y, Wang G, Wank K, and Yang XG. Bis(acetylacetonato)-oxovanadium(iv), bis(maltolato)-oxovanadium(iv) and sodium metavanadate induce antilipolytic effects by regulating hormone-sensitive lipase and perilipin via activation of Akt. *Metallomics*. 2013; 5(7):813-20. https://doi:10.1039/c3mt00001j

Lu L, Saha D, Martuza R, Rabkin S, and Wakimoto H. Single agent efficacy of the VEGFR kinase inhibitor axitinib in preclinical models of glioblastoma. Journal of Neurooncology. 2015; 121(1):91-100. doi:10.1007/s11060-014-1612-1.

Mueller MB, Blunk T, Appel B, Maschke A, Goepferich A, Zellner J, Englert C, Prantl L, Kujat R, Nerlich M, Angele P (2012). Insulin is essential for in vitro chondrogenesis of mesenchymal progenitor cells and influences chondrogenesis in a dose-dependent manner. *International orthopaedics*, *37*(1), 153–158. doi:10.1007/s00264-012-1726-z

Mukherjee, A., & Rotwein, P. (2009). Akt promotes BMP2-mediated osteoblast differentiation and bone development. *Journal of cell science*, *122*(Pt 5), 716–726. doi:10.1242/jcs.042770

National Institute of Health- U.S. National Library of Medicine. Campomelic dysplasia. *Genetics Home Reference*. Reviewed June 2014, Published March 19, 2019. https://ghr.nlm.nih.gov/condition/campomelic-dysplasia

Newton PT, Staines KA, Spevak L, Boskey AL, Teixeira CC, Macrae VE, Canfield AE, Farquharson C. (2012). Chondrogenic ATDC5 cells: an optimised model for rapid and physiological matrix mineralisation. *International journal of molecular medicine*, *30*(5), 1187-93.

Norouzi S, Adulcikas J, Sohal SS, Myers S. Zinc stimulates glucose oxidation and glycemic control by modulating the insulin signaling pathway in human and mouse skeletal muscle cell lines. *PLoS One*. 2018;13(1):e0191727. Published 2018 Jan 26. doi:10.1371/journal.pone.0191727

Ovesen J, Moller-Madsen B, Thomsen JS, Danscher G, and Mosekilde L. The positive effects of zinc on skeletal strength in growing rats. *Bone*. 29(6), 565-70. https://doi.org/10.1016/S8756-3282(01)00616-0

Paglia D, Wey A, Breitbart E, Faiwiszewski J, Siddhant KM, Al-Zube L, Vaidya S, Cottrell JA, Graves D, Benevenia J, O'Connor JP, Lin SS. 2013. The Effects of Local Insulin Delivery on Subperiosteal Angiogenesis and Mineralized Tissue Formation during Fracture Healing. Journal of Orthopedic Research: 31: 783-91.

Patti M and Kahn C. The insulin receptor- a critical link in glucose homeostasis and insulin action. Journal of Basic and Clinical Physiology and Pharmacology. 1998; 9(2-4):89-110. doi.org/10.1515/JBCPP.1998.9.2-4.89.

Peng, H., Wright, V., Usas, A., Gearhart, B., Shen, H. C., Cummins, J., & Huard, J. (2002). Synergistic enhancement of bone formation and healing by stem cell-expressed VEGF and bone morphogenetic protein-4. *The Journal of clinical investigation*, *110*(6), 751–759. doi:10.1172/JCI15153

Pessin J and Saltiel A. Signaling pathways in insulin action: moleculartargets of insulin resistance. Journal of Clinical Investigation. 2000; 106(2): 165-169. https://doi.org/10.1172.JCI10582.

Pirmoradi L, Noorafshan A, Safaee A, Dehghani GA. Quantitative Assessment of Proliferative Effects of Oral Vanadium on Pancreatic Islet Volumes and Beta Cell Numbers of Diabetic Rats. *Iran Biomed J*. 2016;20(1):18–25. doi:10.7508/ibj.2016.01.003

Sakurai H, Kojima Y, Yoshikawa Y, Kawabe K, and Yasui H. Antidiabetic vanadium(IV) and zinc(II) complexes). Coordination Chemistry Reviews. 2002; 226(1-2), 187-198. doi:10.1016/s0010-8545(01)00447-7

Saltiel A and Kahn C. Insulin signaling and the regulation of glucose and lipid metabolism. Nature. 2001; 414:799-806. Retrieved from https://www.nature.com/articles/414799a

Sanchez-Elsner T, Botella LM, Velasco B, Corbi A, Attisano L, Bernabeu C. Synergistic cooperation between hypoxia and transforming growth factor-beta pathways on

human vascular endothelial growth factor gene expression. J Biol Chem, 2001; 276: 38527-35.

Sekiya I, Colter DC, and Prockop DJ. BMP-6 enhances chondrogenesis in a subpopulation of human marrow stromal cells. Biochemical and Biophysical Research Communications. 2001; 284(2). 411-418. https://doi.org/10.1006/bbrc.2001.4898

Sfeir C, Ho L, Doll BA, Azari K, Hollinger JO. Fracture repair. In: Lieberman JR, Friedlaender GE, editors. Bone regeneration and repair. Humana Press; Totowa, NJ: 2005. pp. 21–44.

Shapiro I, DeBolt K, Funanage V, Smith S, Tuan R. Developmental regulation of creatine kinase activity in cells of the epiphyseal growth plate. J. Bone Miner. Res. 1992;7:493–500.

Sosic D, Brand-Saberi B, Schmidt C, Christ B, Olson E. Regulation of *paraxis* expression and somite formation by ectoderm- and neural tube-derived signals. Dev. Biol. 1997;185:229–243.

Tsuji K, Bandyopadhyay A, Harfe BD, Cox K, Kakar S, Gerstenfeld L, Einhorn T, Tabin CJ, Rosen V. BMP2 activity, although dispensable for bone formation, is required for the initiation of fracture healing. Nature Genetics. 2006;38(12):1424–9.

Tudor R, Zalewiski P, and Ratnaike R. Zinc in health and chronic disease. Journal of Nutrition, Health, and Aging. 2005; 9(1), 45-51

Vardatsikos G, Pandey N, and Srivastava A. Insulino-mimetic and anti-diabetic effects of zinc. Journal of Inorganic Biochemistry. 2013; 120,8-17. doi:10.1016/j.jinorgbio.2012.11.006

Wang, Wenhao & Yeung, Kelvin. (2017). Bone grafts and biomaterials substitutes for bone defect repair: A review. Bioactive Materials. 2. 10.1016/j.bioactmat.2017.05.007.

Wendeberg B. Acta Orthopaedica. 52. 1961. Mineral metabolism of fractures of the tibia in man studied with external counting of Sr85; pp. 1–79.

Wey A, Cunningham C, Hreha J, Breitbart E, Cottrell J, Ippolito J, Clark D, Lin H, Benevenia J, O'Connor J, Lin S, and Paglia D. Local $ZnCl_2$ accelerates fracture healing. *Journal of Orthopaedic Research*. 2014; 32(6), . https://doi.org/10.1002/jor.22593

Wright E, Hargrave M, Christiansen J, Cooper L, Kun J, Evans T, Gangadharan U, Greenfield A, Koopman P. The Sry-related gene *Sox9* is expressed during chondrogenesis in mouse embryos. Nature Genet. 1995; 9:15–20.

Wu L N, Genge B R, Dunkelberger D G, LeGeros R Z, Concannon B, Wuthier R E. Physiochemical characterization of the nucleational core of matrix vesicles. J. Biol. Chem. 1997; 272:4404–4411.

Yang F, Xue F, Guan J, Zhang Z, Yin J, and Kang Q. Stromal-Cell-Derived Factor (SDF) 1-Alpha Overexpression Promotes Bone Regeneration by Osteogenesis and Angiogenesis in Osteonecrosis of the Femoral Head. *Cellular Physiology and Biochemistry*. 2018; 46(6), 2561-75. https://doi.org/10.1159/000489684

Yang J, Andre P, Ye L, Yang YZ. The Hedgehog signalling pathway in bone formation. *Int J Oral Sci*. 2015;7(2):73-9. Published 2015 May 29. doi:10.1038/ijos.2015.14

Yang X, Ricciardi BF, Hernandez-Soria A, Shi Y, Pleshko Camacho N, Bostrom MP. Callus mineralization and maturation are delayed during fracture healing in interleukin-6 knockout mice. Bone. 2007;41(6):928–36.

Zelzer E, Levy Y, Kahana C, Shilo BZ, Rubinstein M, Cohen B. Insulin induces transcription of target genes through the hypoxia-inducible factor HIF-1α/ARNT. EMBO J, 1998;17: 5085-94.

Zhang, J. M., & An, J. (2007). Cytokines, inflammation, and pain. *International anesthesiology clinics*, *45*(2), 27–37. doi:10.1097/AIA.0b013e318034194e

Appendix 1

Sample Name and Timepoint	**A260/A280**	**Concentration (ug/uL)**
Growth Media 1 Day 1	2.019	0.546ug/uL
Growth Media 2 Day 1	2.013	0.773
Growth Media 3 Day 1	2.029	0.733
Insulin 1 Day 1	2.016	0.834
Insulin 2 Day 1	2.036	0.903
Insulin 3 Day 1	2.026	0.928
$ZnCl_2$ 1 Day 1	2.023	0.243
$ZnCl_2$ 2 Day 1	2.042	0.245
$ZnCl_2$ 3 Day 1	2.029	0.273
Growth Media 1 Day 4	2.040	0.230
Growth Media 2 Day 4	2.044	0.398
Growth Media 3 Day 4	2.039	0.370
Insulin 1 Day 4	2.051	0.365
Insulin 2 Day 4	2.045	0.420
Insulin 3 Day 4	2.036	0.393
$ZnCl_2$ 1 Day 4	2.008	0.228
$ZnCl_2$ 2 Day 4	2.029	0.314
$ZnCl_2$ 3 Day 4	2.047	0.308
Growth Media 1 Day 7	1.992	0.333

Growth Media 2 Day 7	2.058	0.506
Growth Media 3 Day 7	2.065	0.408
Insulin 1 Day 7	2.053	0.511
Insulin 2 Day 7	2.046	0.393
Insulin 3 Day 7	2.051	0.507
$ZnCl_2$ 1 Day 7	2.050	0.364
$ZnCl_2$ 2 Day 7	2.054	0.394
$ZnCl_2$ 3 Day 7	2.048	0.400
Growth Media and 1uM Axitinib 1 Day 1	2.017	0.611
Growth Media and 1uM Axitinib 2 Day 1	2.028	0.672
Growth Media and 1uM Axitinib 3 Day 1	2.029	0.693
Insulin and 1uM Axitinib 1 Day 1	2.022	0.758
Insulin and 1uM Axitinib 2 Day 1	2.033	0.795
Insulin and 1uM Axitinib 3 Day 1	2.037	0.853
$ZnCl_2$ and 1uM Axitinib 1 Day 1	2.022	0.177
$ZnCl_2$ and 1uM Axitinib 2 Day 1	2.026	0.251
$ZnCl_2$ and 1uM Axitinib 3 Day 1	2.014	0.202

Growth Media and 1uM Axitinib 1 Day 4	2.023	0.462
Growth Media and 1uM Axitinib 2 Day 4	2.021	0.472
Growth Media and 1uM Axitinib 3 Day 4	2.028	0.477
Insulin and 1uM Axitinib 1 Day 4	2.031	0.355
Insulin and 1uM Axitinib 2 Day 4	2.035	0.390
Insulin and 1uM Axitinib 3 Day 4	2.036	0.318
$ZnCl_2$ and 1uM Axitinib 1 Day 4	2.048	0.233
$ZnCl_2$ and 1uM Axitinib 2 Day 4	2.013	0.321
$ZnCl_2$ and 1uM Axitinib 3 Day 4	2.014	0.270
Growth Media and 1uM Axitinib 1 Day 7	2.044	0.533
Growth Media and 1uM Axitinib 2 Day 7	2.048	0.499
Growth Media and 1uM Axitinib 3 Day 7	2.051	0.445
Insulin and 1uM Axitinib 1 Day 7	2.043	0.365
Insulin and 1uM Axitinib 2 Day 7	2.049	0.384

Insulin and 1uM Axitinib 3 Day 7	2.046	0.371
$ZnCl_2$ and 1uM Axitinib 1 Day 7	2.048	0.202
$ZnCl_2$ and 1uM Axitinib 2 Day 7	2.059	0.465
$ZnCl_2$ and 1uM Axitinib 3 Day 7	2.047	0.515

Table 7: RNA quality and concentration analysis.

Appendix 2

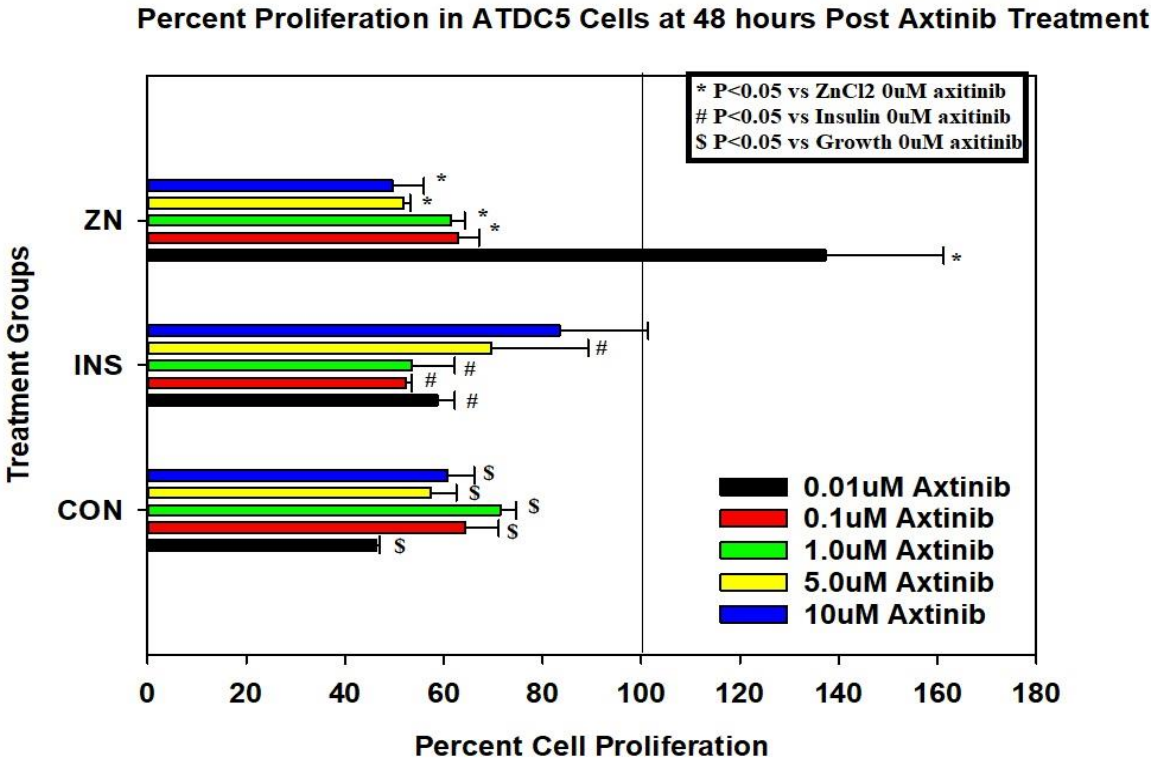

Figure 11: Cellular Proliferation in ATDC5 Cells at 48hours Post Axitinib Treatment Dose Dependent Response in an MTT Assay.

This figure demonstrates treatment groups $ZnCl_2$ (ZN), insulin (INS), and growth media (CON) and their cellular proliferation after being exposed to various doses of

Axitinib. A vertical line at 100% shows the proliferation rate of cells without Axitinib. In this figure, every dosage of the Axitinib caused a statistically significant decrease in cellular proliferation except for $ZnCl_2$ 0.01uM.

Appendix 3